NASA CR-112080

NAS1-10564

FINAL REPORT

FABRICATION AND EVALUATION OF A WEAK ZONE PLATE FOR MONITORING PERFORMANCE OF LARGE ORBITING TELESCOPES

BY: DR. KENT E. ERICKSON

PREPARED UNDER CONTRACT NAS1-10564

KEUFFEL & ESSER COMPANY
MORRISTOWN, NEW JERSEY

NATIONAL AERONAUTICS & SPACE ADMINISTRATION
LANGLEY RESEARCH CENTER
HAMPTON, VIRGINIA

JULY 15, 1972

NAS1-10564

FINAL REPORT

FABRICATION AND EVALUATION OF A WEAK ZONE PLATE FOR MONITORING PERFORMANCE OF LARGE ORBITING TELESCOPES

BY: DR. KENT E. ERICKSON

PREPARED UNDER CONTRACT NAS1-10564

KEUFFEL & ESSER COMPANY
MORRISTOWN, NEW JERSEY

NATIONAL AERONAUTICS & SPACE ADMINISTRATION
LANGLEY RESEARCH CENTER
HAMPTON, VIRGINIA

JULY 15, 1972

TABLE OF CONTENTS

FIGURES

1.0 SUMMARY

An experimental study has been made of the feasibility of monitoring the optical performance of a large telescope by means of a very faint phase hologram imprinted upon the primary mirror. Tests have been made using an f/5 telescope with a 0.3 m aperture. The results indicate that a usable hologram can be so faint and so restricted in area that it will probably not interfere significantly with normal operation of a 3.0 m telescope at wavelengths longer than 100 nm for stars brighter than magnitude 29.

2.0 INTRODUCTION

The work reported herein is an outgrowth of a proposal by K&E, April 1966, for a holographic focal plane technique of monitoring the optical performance of large telescopes. The present contract is a sequel to contract NASW-1856, the results of which are reported in NASA CR-111811.

The technique under investigation involves the use of a zone pattern imprinted in very light relief upon the surface of the primary mirror. Under contract NASW-1856 encouraging results were obtained with a zone relief of $\lambda/4$ (@ λ = 633 nm). The present contract was aimed at demonstrating the feasibility of using a relief height of $\lambda/100$ or less.

Specific objectives of the present contract are:

1. To improve the technique of generating a weak zone pattern upon a telescope objective, the design goal being a diffraction efficiency of 0.1% or less.
2. To combine the primary mirror (with zone pattern impressed) with a suitable secondary and interferometer into a model to demonstrate the feasibility of the zone pattern technique.
3. To evaluate the concept to show the effect of the zone pattern on the normal operation of the telescope.

It is recognized that the most practical means of generating a zone pattern on a very large mirror may be to scribe the zones with a "laser stylus" under interferometric control. Budgetary limitations, however, necessarily restricted the present study to zone patterns which are generated holographically.

3.0 SYMBOLS

a = Zone period.

b = Width of the half-zones of Type A (see Figure 2).

D = Diameter of the primary mirror.

f = F/D = Aperture ratio of the primary mirror.

F = Focal length of the primary mirror.

I_o = Average illuminance within the Airy disc.

I_{+1} = Illuminance due to first order diffracted light.

I_s = Illuminance due to scattered light.

m_o = Magnitude of the zero order stellar image.

m_{+1} = Magnitude of the first order light diffracted into a cone equal to that of the Airy disc.

m_s = Magnitude of the light diffracted into a cone equal to that of the airy disc.

N = Order of diffraction at wavelength λ_o.

N' = Order of diffraction for starlight.

t = Deposited thickness of the relief layer.

t' = Effective step height of the zones.

$\left.\begin{matrix}\alpha \\ \beta\end{matrix}\right\}$ = Holographic parameters (see Figures 4 & 5).

ϵ_N = Nth order diffraction efficiency.

ϵ_λ = Total diffraction efficiency for all orders ($N \neq 0$) combined.

$\bar{\epsilon}_\lambda$ = Effective diffraction efficiency for galactic radiation.

η = Width of Type B sub-zones relative to Type A half-zones (see Figures 2 & 3).

$\gamma = \lambda'/\lambda_o$

λ_o = Wavelength of the monitoring light

λ' = Wavelength of the holographic source

λ = Wavelength of starlight

Other symbols are defined where they are used.

4.0 BRIEF DESCRIPTION OF THE MONITORING TECHNIQUE

4.1 Basic Technique

The monitoring technique studied in this contract is a holographic technique which provides information as to the total performance (figure, alignment and focus) of the primary mirror.

The technique is illustrated in Figure 1. An interferometer with a laser souce is located at the focal plane of the telescope. The laser emits a uniphase wave front which is divided into a "monitoring wave" and a "reference wave". Most of the "monitoring wave" is directed toward the stars and is lost. A small portion, however, is diffracted by the weak zone pattern (reflection phase hologram) on the primary mirror and returns through the telescope where it is recombined with the reference wave to form an interference pattern at an image of the primary mirror. The phases of this interference pattern are sampled at an array of points. The sampled values ϕ_i are compared with a set of phase values ϕ_i' which correspond to perfect figure, alignment and focus of the primary mirror.

4.2 Automated Sensing and Control

In the present investigation, the interference pattern was recorded photographically. For use with a control system, it would, of course, be necessary to use photodetectors.

Figure 1 shows how automatic sensing might be done. An array of sensors located at the image of the primary mirror senses variations in the intensity of the interference pattern. A frequency shifter in the reference beam converts spatial phase information into temporal phase information. The phases ϕ_i of the electrical signals are compared with a corresponding set of desired values ϕ_i' stored in memory. The control system may then actively control

TELESCOPE MONITORING & CONTROL SCHEMATIC

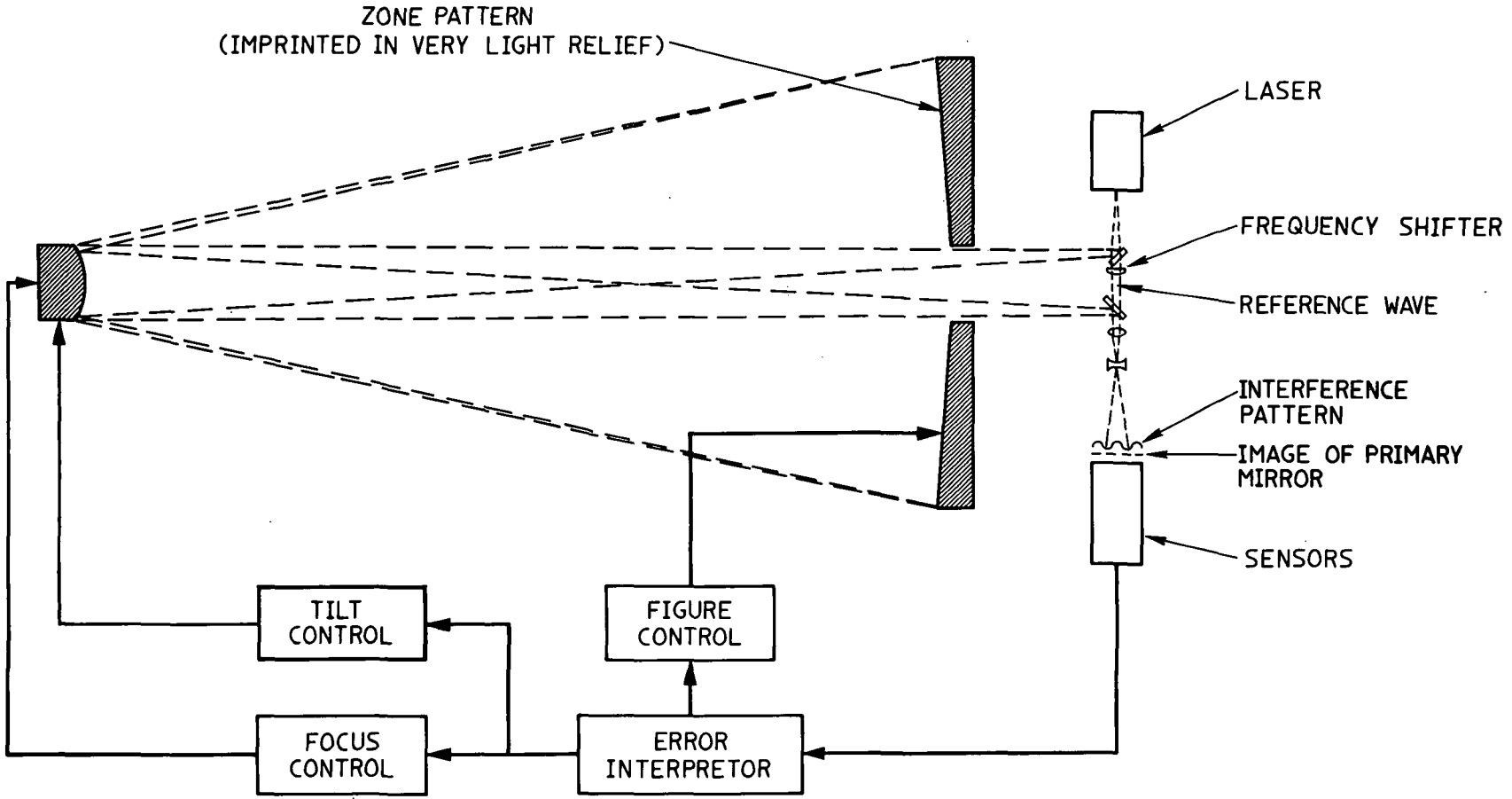

FIGURE 1

the figure, alignment and focus of the optics so as to maintain the condition $\phi_i = \phi_i'$. A more complete discussion is given in Section 13.4.

4.3 Nature of the Zone Pattern

A circular zone pattern is imprinted in low relief upon the surface of the primary mirror. The mirror surface is overcoated to give uniform reflectivity. In modern terminology this is a "reflection phase hologram".

The zone period must vary radially in such a manner as to focus one diffraction order back through the telescope. The condition for this is:

$$a_r = 2 N f_r \lambda_o \tag{1}$$

where:

a_r = Zone period at a zone of radius r.

N = Order of diffraction.

f_r = Aperture ratio of the mirror at a zone of radius r.

λ_o = Wavelength of the monitoring light.

In the present investigation:

$f_{(min)} = 5$

$N = 1$

$\lambda_o = .633\ \mu m$

This resulted in a minimum zone period at the periphery of the mirror of:

$$a_{min} = 6.33 \mu m \tag{2}$$

There are two options for limiting the diffraction efficiency of the zones so as to limit their effect upon normal operation of the telescope:

Option (A): The step height of the zones may be limited.
Option (B): The number of zones and the width of each raised (or lowered) subzone may be limited.

DIFFRACTION LOSS FROM TYPE A ZONES

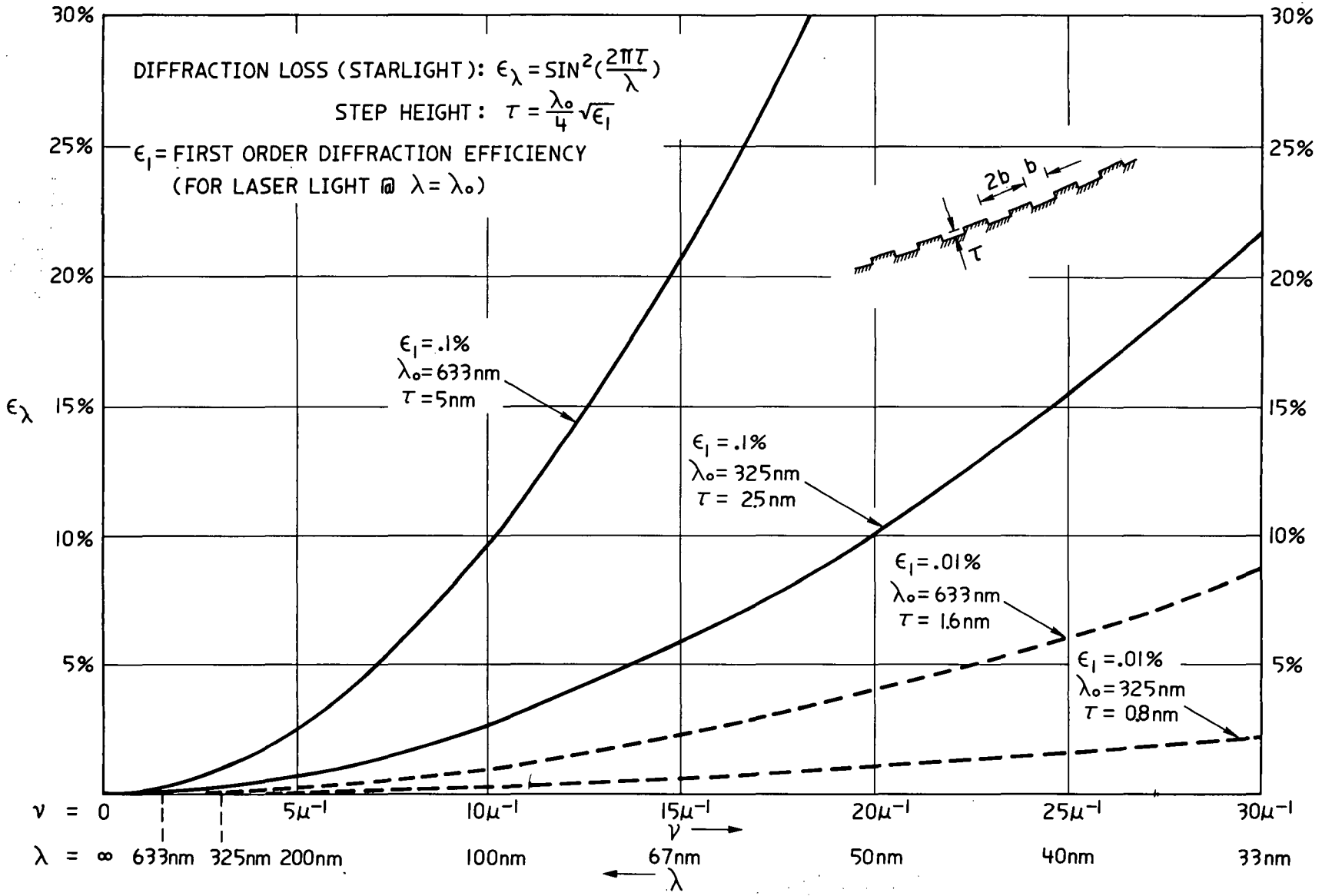

FIGURE 2

DIFFRACTION LOSS FROM TYPE B ZONES

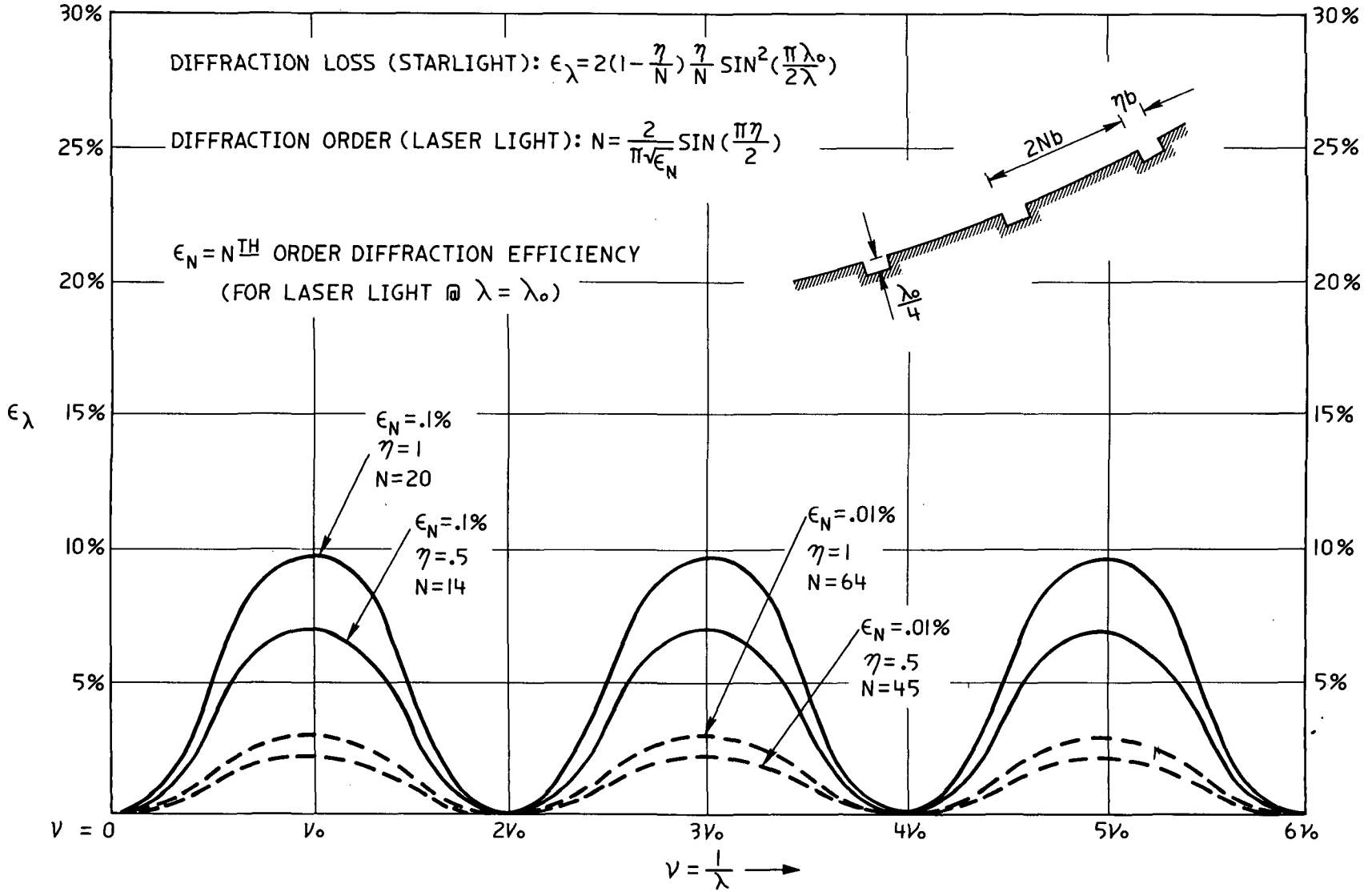

FIGURE 3

Figures 2 and 3 show how the diffraction loss of starlight depends upon wavelength and zone geometry. Figure 2 applies to Option (A) and Figure 3 applies to Option (B). The analysis may be found in Section 13.2.

Option (A) was used exclusively in the present investigation since it is the only practical alternative when the zones are generated photographically.

5.0 GENERATION OF THE ZONE PATTERN

5.1 Holographic Arrangement

The period of the zone pattern must vary radially in such a manner as to return the first order diffracted wave back to the prime focus of the mirror. Figure 4 illustrates the geometry for generating such a pattern holographically by photographing the interference between two coherent waves.

Ideally one wave should diverge from the prime focus of the mirror and the other wave should be a plane wave approaching on axis, both waves having the same wavelength λ_o as that to be used for monitoring the performance of the telescope. Practically, however, it is difficult to generate a truly plane wave over a large aperture. It is fortunate, therefore, that a nearly identical pattern can be generated using the compromise geometry shown in Figure 4 provided the wavelength is shortened from λ_o to some smaller value λ'. Derivations of the formulae for parameters α and β (defined in Figure 4) are given in Section 13.3.

The holographic arrangement is shown in Figures 5 and 6. The parameters used were

$$\lambda' = 488 \text{ nm}$$

$$\lambda_o = 632 \text{ nm}$$

$$F = 60 \text{ in}$$

$$\alpha = 3.10$$

$$\beta = .966$$

The output of the argon laser was approximately .3 watt TEM_{oo}.

Holographic parameters α and β were not precisely adjusted, hence several fringes of spherical aberration appear in the interferograms in Figures 13, 14, 15, 16.

HOLOGRAPHIC ZONE PATTERN GENERATION

IDEAL GEOMETRY

Two coherent sources; wavelength λ_o

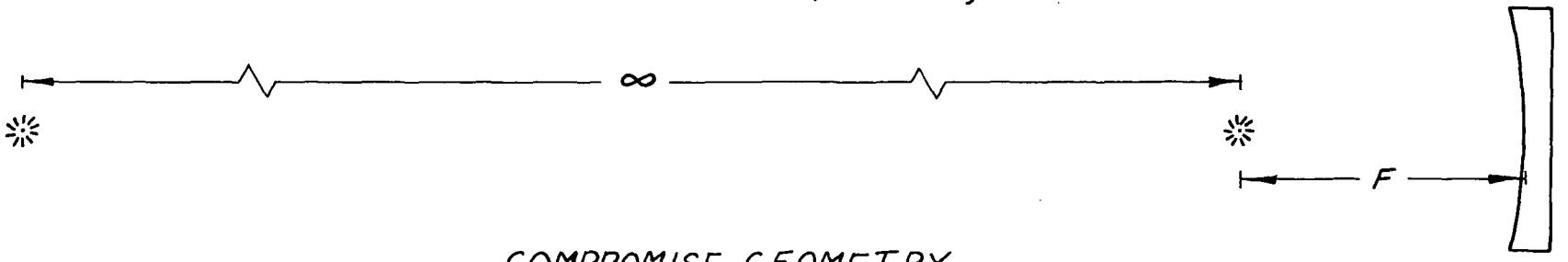

COMPROMISE GEOMETRY

Two coherent sources; wavelength $\lambda' < \lambda_o$

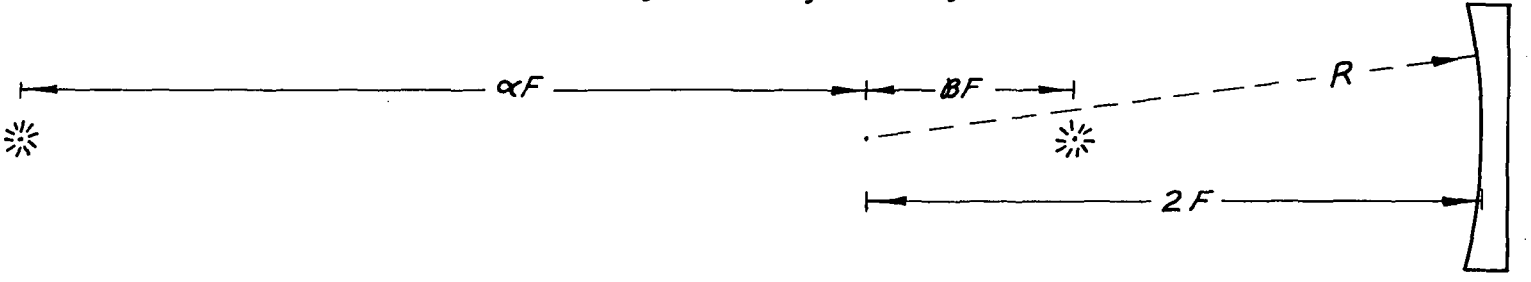

$$\alpha = \frac{4\gamma^2 - \gamma - 2 + \sqrt{4 - 3\gamma^2}}{2\gamma(1-\gamma)} \qquad \beta = \frac{4\gamma^2 + \gamma - 2 + \sqrt{4 - 3\gamma^2}}{2\gamma(1+\gamma)} \qquad \left[\gamma \equiv \frac{\lambda'}{\lambda_o}\right]$$

FIGURE 4

HOLOGRAPHIC ZONE PATTERN GENERATOR

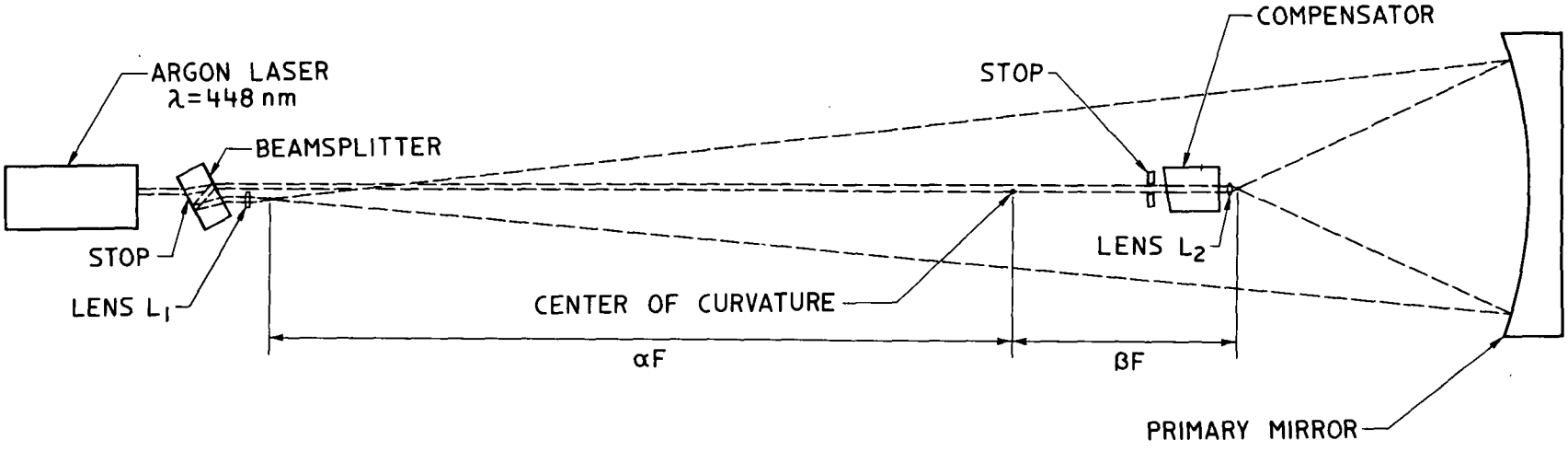

FIGURE 5

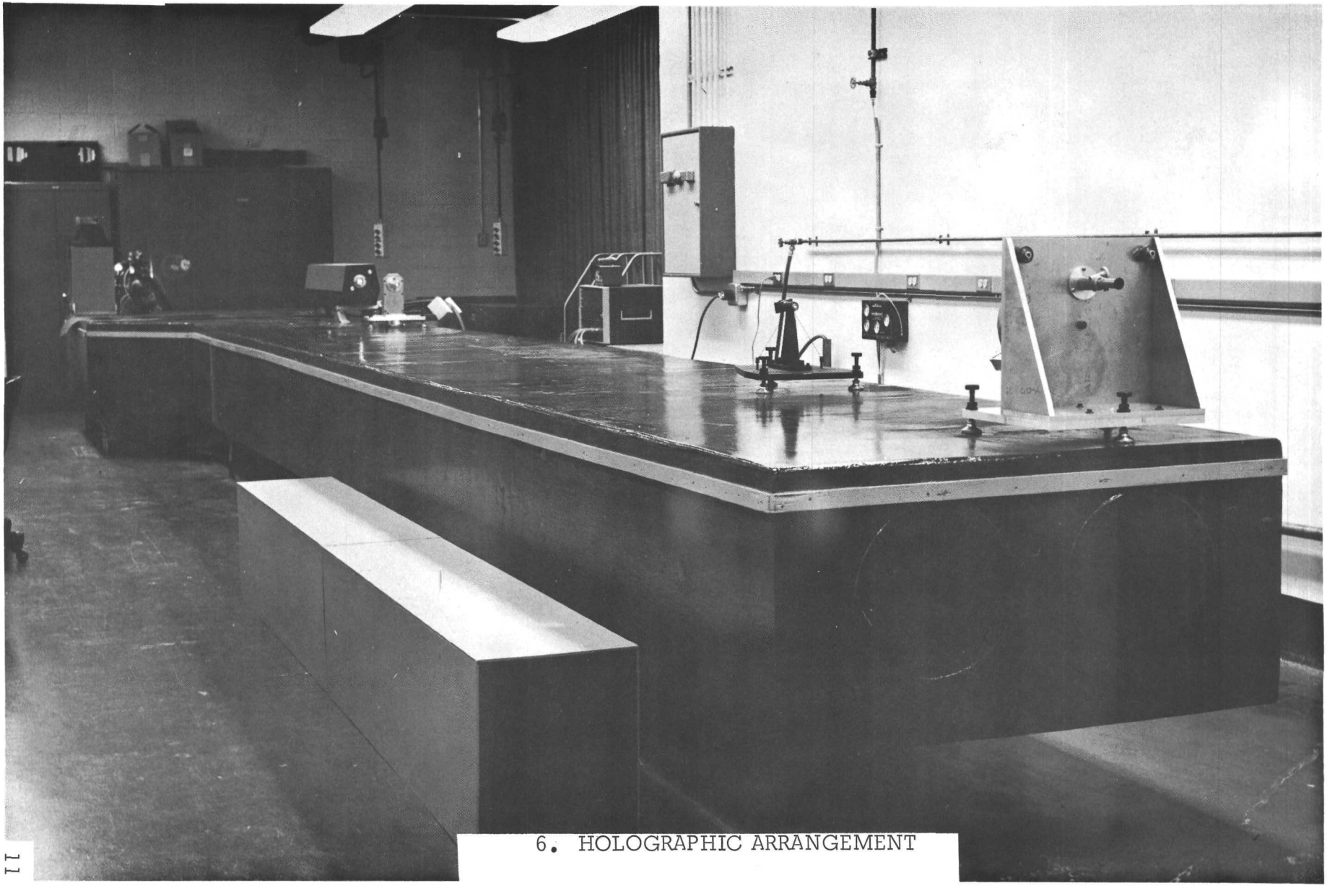

6. HOLOGRAPHIC ARRANGEMENT

5.2 Mirrors

The results in this investigation were obtained principally from two mirrors, designated in this report as Mirror #1 and Mirror #2.

Mirror #1 was imprinted with a zone pattern over essentially the entire aperture.

Mirror #2 was imprinted with a zone pattern restricted by a mask (Figure 7).

Both mirrors were of "Cer-Vit":

Diameter: D = 12"
Aperture Ratio: f = 5
Overcoating: Aluminum

5.3 Photographic Procedure

Kodak KOR photoresist was used as the photosensitive material. Two basic techniques were tried:

(a) The zones were etched into a layer beneath the developed photoresist image.
(b) The zones were built up by deposition of material after development of the photoresist image.

The second method was eventually adopted because it gave more uniform results and permitted the use of highly stable materials (e.g., quartz) for the relief pattern.

5.3.1 Substrate Preparation

Before coating with KOR, the mirror surface was first coated with an opaque layer of chrome followed by a layer of SiO_2 85 nm thick. The chrome layer protected the photoresist against light scattered from the rear. Light reflected from the chrome in combination with the incident light generated a standing wave having a node near the surface of the chrome. Consequently, without the SiO_2 layer the KOR tended to be underexposed at the KOR/chrome interface resulting in poor adherence of the KOR. The function of the SiO_2 layer was to locate the bonding face of the KOR layer at a region of high light intensity (i.e., in the vicinity of an anti-node of the standing wave).

5.3.2 Photoresist Coating

A satisfactory coating was produced by whirling under the following conditions:

Dilution: 10 parts KOR thinner to 1 part KOR.
Temperature: 22°C
Acceleration: 0 to 675 rpm in 15 seconds.

To minimize streaking, the blank was completely flooded before whirling.

5.3.3 Exposure

A 2 1/2 minute exposure at an illuminance of approximately 0.4 watt/m^2 was found to be satisfactory.

5.3.4 Development

(a) The image was soaked in KOR Developer (@ 72°F) for 4 minutes with gentle agitation.

(b) The fringe pattern was developed immediately with KOR developer. Considerable hydraulic action was needed. It proved desirable to use a sprayer which could apply a forceful spray to a large area so as to facilitate uniform development. (WARNING: Do not breathe vapors from KOR Developer.)

(c) The developed pattern was spray rinsed with xylene.

5.3.5 Zone Deposition

(a) The surface was cleaned for 5 minutes with a glow discharge. The discharge was operated at a pressure of .1 mm Hg and a current of approximately 50 milliamperes using a 12" diameter ring cathode located 10" from the mirror surface.

(b) A layer of SiO_2 of the thickness desired for the zone step height was deposited on the surface. (See Section 6 for the calibration procedure.)

5.3.6 Photoresist Removal

Removal of the photoresist without damage to the zones proved to be the most troublesome aspect of the entire photographic process. The only suitable technique which was found for removing the photoresist without abrasion was to fire it off at a temperature of 400°C. This, too, proved unsatisfactory in areas which were pre-exposed to room light in order to suppress the zone pattern (see Section 5.3.7). At the completion of the experiments it was found that prolonged exposure to the glow discharge might have been a better procedure for removal of the photoresist.

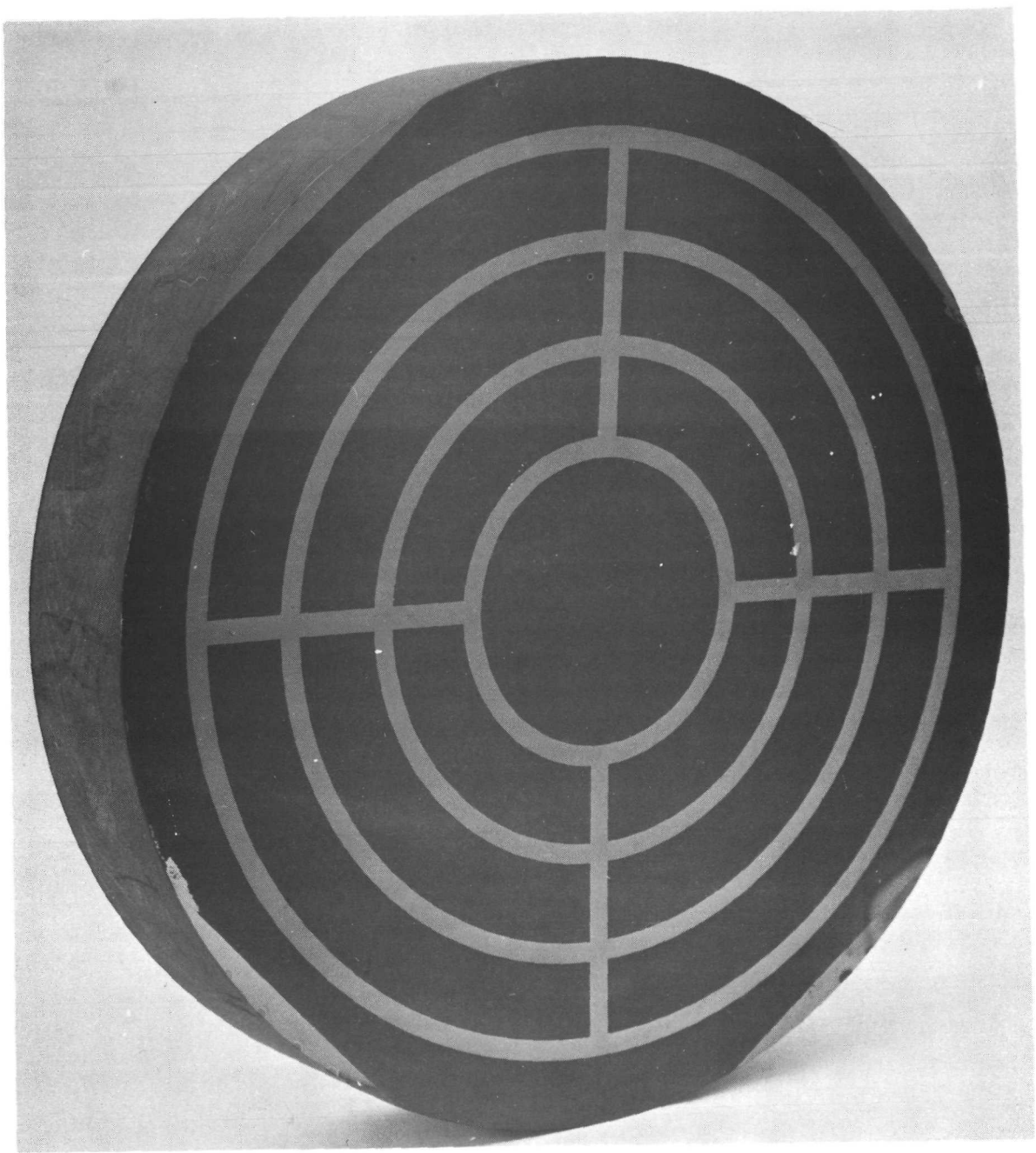

7. MASK

5.3.7 Masking

In those areas in which it was desired that the relief pattern be suppressed, the photoresist was pre-exposed before being exposed to the fringe pattern. The mask used for this pre-exposure is shown in Figure 7. This technique appeared to be successful until the mirror was subjected to a very vigorous cleaning. It then appeared that the photoresist in the pre-exposed areas had not been removed by baking at 400°C. The cleaning brought out the latent fringe pattern in the resist layer. As may be seen in Figure 17 this occurred principally toward the center of the mirror where the fringes are broadest. Even the most diligent cleaning with hot strippers failed to remove the resist in the pre-exposed areas. The pre-exposure technique is therefore not recommended. In any future experimentation of this sort it would be preferable to mask out the unwanted areas with aluminum prior to deposition of the resist.

6.0 MEASUREMENT OF ZONE STEP HEIGHT

A zone step height of 100 Å or less is too small to be measured accurately by direct interferometric means. The thickness of the layer which formed the step was therefore measured using a quartz crystal monitor.

To calibrate the quartz crystal monitor for very thin layers, a thick layer was built up to 20 layers. Each layer was identical in composition and in frequency reading to the relief layer that was deposited on the mirror designated in this report as Mirror #1. Evaporation was stopped and the crystal frequency was re-zeroed after the deposition of each layer. The composite layer occupied a strip through the center of the test sample as shown in Figure 8. The thickness of the composite layer was determined by measuring the offset of the Fizeau fringes in Figure 8.

The above calibration showed that the step height of SiO_2 initially deposited upon Mirror #1 was:

$$t = 8.4 \text{ nm} \tag{3}$$

The effective step height, t' , that remained on Mirror #1 after removal of the photoresist was calculated from the following relation between effective step height t' and the first order diffraction efficiency ϵ_1 :

$$t' = \frac{\lambda}{4}\sqrt{\epsilon_1} \tag{4}$$

Relation (4) is for a zone pattern with a regular "square wave" profile (see Section 13.2.1, Relation (41)).

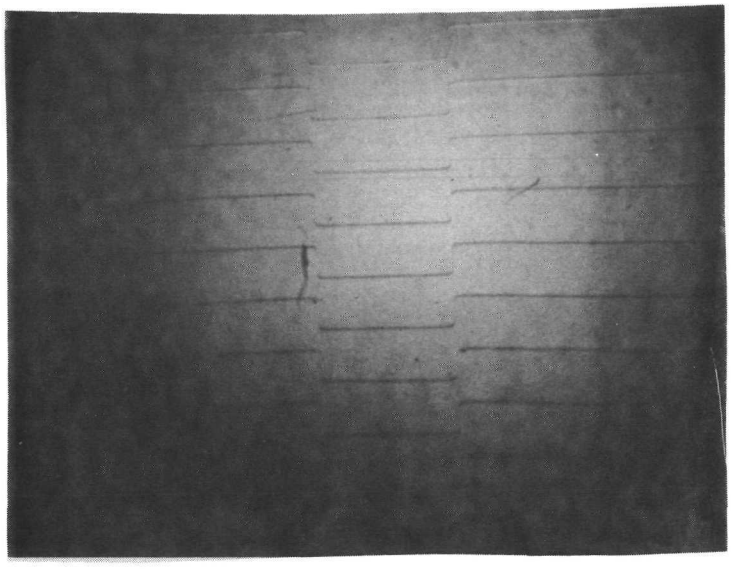

8. STEP HEIGHT CALIBRATION

Substitution into (4) of the values for λ and ϵ_1 in Section 7.2 yields the following value for the effective step height t':

$$t' = 2.4 \text{ nm} \qquad (5)$$

Some reduction was expected between the calibrated step height t and the effective step height t' since the profile of the zones was not perfectly regular, the width of the raised zones being on the average about 50% greater than that of the unraised zones. Also abrasion of the raised zones undoubtedly occurred during the vigorous cleansing required for removal of the photoresist. The magnitude of the difference however, was unexpectedly large. The probable reason emerged only when a masked pattern was generated on Mirror #2. In this masking process, certain areas were pre-exposed through the mask (Figure 7) in order to suppress the relief pattern. Contrary to expectations, the photoresist in these pre-exposed areas was not removed by elevating the temperature to 400°C, nor could it be removed thereafter even by the most diligent cleansing (see Section 5.3.6). In view of the tenacity of the photoresist in the pre-exposed areas, it appears likely that the baking at 400°C left a residue a few nanometers thick in the areas that were not pre-exposed, thus reducing the effective step height of the bare SiO_2 zones.

7.0 MEASUREMENT OF DIFFRACTION EFFICIENCY

7.1 Procedure

A measurement was made of the first order diffraction efficiency of the mirror designated in this report as Mirror #1. This measurement was made by placing a silicon photocell at the focus of the +1 diffraction order in the arrangement shown in Figure 9. The power detected at this focus was compared with the power detected at the zero order focus. The power at the zero order focus was measured with the same photocell but with a calibrated attenuator in the beam to prevent saturation.

7.2 Results

The first order diffraction efficiency measured by the above procedure was:

$$\epsilon_1 = .040\% \qquad (\lambda = 488 \text{ nm}) \qquad (6)$$

The diffraction efficiency varies as the inverse square of the wavelength. Hence, in the telescope monitor (which has a He-Ne source), the calculated first order diffraction efficiency of Mirror #1 is:

$$\epsilon_1 = .024\% \qquad (\lambda = 633 \text{ nm}) \qquad (7)$$

DIFFRACTION AND SCATTER TEST SCHEMATIC

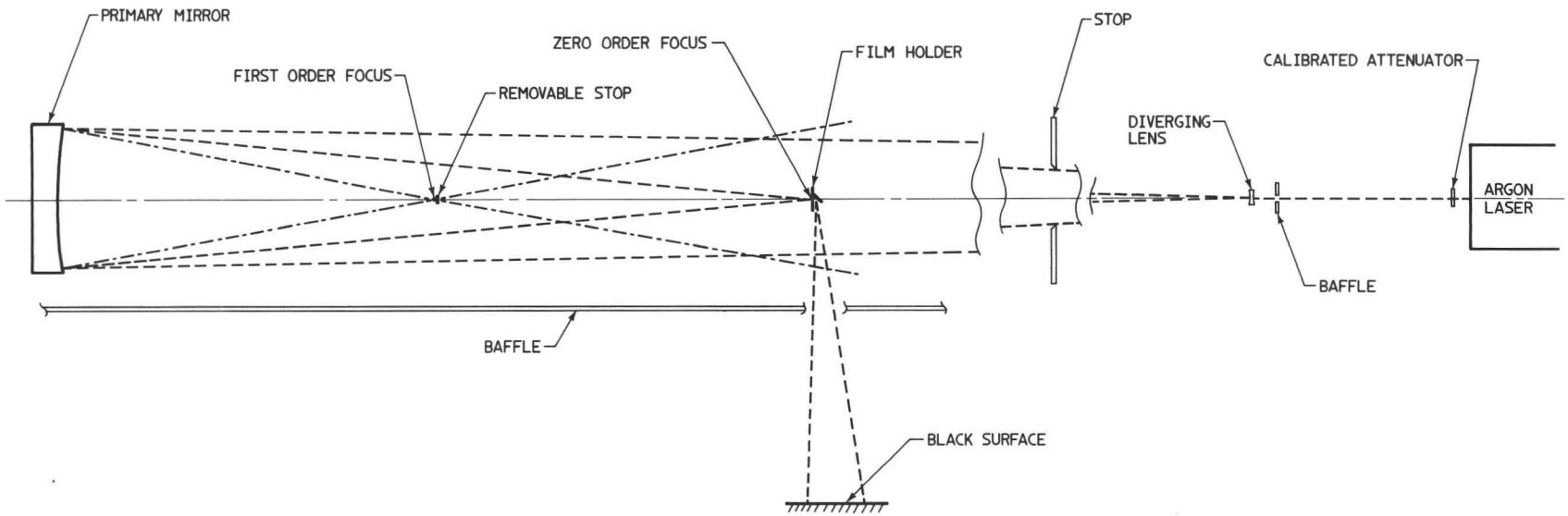

FIGURE 9

Assuming a regular "square wave" relief profile for the zones, the total diffraction efficiency ϵ for all diffraction orders ($N \neq 0$) is given by the following relation (see Section 13.2.1, Relation (42)):

$$\epsilon_\lambda = \left(\frac{\pi}{2}\right)^2 \epsilon_1 \tag{8}$$

Hence, for Mirror M_1:

$$\epsilon_\lambda = .059\% \qquad (\lambda = 633 \text{ nm}) \tag{9}$$

7.3 Discussion

The first order diffracted light subtends a cone in the field of view of the telescope which has an angular diameter θ given by:

$$\theta \approx \frac{1}{f} \tag{10}$$

The Airy disc of a stellar image subtends a cone in the field of view of the telescope which has an angular diameter θ' given by:

$$\theta' = \frac{2.44\,\lambda}{D} \tag{11}$$

If it is assumed that all the diffracted light reaches the focal plane, the ratio in intensity between the in-focus zero order light I_0 and the out-of-focus first order light I_{+1} is given by:

$$\frac{I_{+1}}{I_0} \approx \epsilon_1 \left(\frac{\theta'}{\theta}\right)^2 \tag{12}$$

Substitution of (10) and (11) into (12) gives:

$$\frac{I_{+1}}{I_0} \approx \epsilon_1 \left(\frac{2.44\, f \lambda}{D}\right)^2 \tag{13}$$

But from Relation (4) of Section 6:

$$\epsilon_1 \lambda^2 = (4t')^2 \tag{14}$$

where t' = effective step height.

Substitution of (14) into (13) gives:

$$\frac{I_{+1}}{I_0} \approx \left(\frac{9.76\, t' f}{D}\right)^2 \tag{15}$$

In terms of stellar magnitudes;

$$m_{+1} - m_0 \approx -2.5 \, Log\left[\frac{I_{+1}}{I_0}\right] \tag{16}$$

where:

m_0 = magnitude of the zero order image

m_{+1} = magnitude of the first order diffracted light falling within an area equal to that of the Airy diffraction disc.

Substitution of (15) into (16) gives:

$$m_{+1} - m_0 \approx 5 \, Log\left[\frac{D}{9.76\, t' f}\right] \tag{17}$$

Since m_{+1} and m_0 both refer to the same star, Relation (17) is independent of λ .
The effective values for Mirror #1 were:

D = .300 m

t' = 2.4 nm

Substitution of these values into (17) gives:

$$m_{+1} - m_0 \approx 32.0 \text{ magnitudes} \tag{18}$$

From any given locality on the primary mirror, diffraction orders +1 and -1 cannot both reach the focal plane simultaneously. Indeed, for the on-axis position of a star and for most off-axis positions as well, neither the +1 nor the -1 diffraction orders (nor the less intense higher orders) will reach the focal plane. Therefore, in view of the fact that Mirror #1 by no means represents the practical lower limit for diffraction, it appears that background due to diffraction from a single bright star will not be a serious problem. This is in agreement with the analysis in Section 2.1.3.1 of Report NASA CR-111811. It should also be noted (as shown by Relation (17)) that the intensity of the diffracted background relative to the intensity of stellar images decreases with increasing diameter D of the telescope.

In the case of galactic radiation from many stars combined, it appears that the analysis in Section 2.1.3.2.2 of Report NASA CR-111811 was conservative, being based on an effective diffraction efficiency $\bar{\epsilon}_\lambda$ for galactic radiation of:

$$\bar{\epsilon}_\lambda < 10\%$$

The present results indicate that a diffraction efficiency $\epsilon_1 < .01\%$ should suffice for monitoring purposes. Therefore, according to Figure 2, a reasonable estimate of $\bar{\epsilon}_\lambda$ in the spectral region above 100 nm is:

$$\bar{\epsilon}_\lambda < 1\% \tag{19}$$

This reduction in the upper bound of $\bar{\epsilon}_\lambda$ changes the estimate of the effective magnitude of the background due to diffracted galactic radiation from M' > 29.5 magnitude to:

$$M' > 32 \text{ magnitudes} \tag{20a}$$

(i.e., the background intensity from diffracted galactic radiation is not expected to exceed the average intensity in the Airy disc of a star of magnitude 32).

To be conservative, we shall assume a value:

$$M' > 30 \text{ magnitudes} \tag{20b}$$

8.0 INTERFERENCE TESTS

Interference tests were performed to help answer two questions:
(1) Is it possible to monitor telescope performance using a zone pattern so faint as to have substantially no effect upon the normal performance of the telescope?
(2) Is it practical to restrict the zone pattern to relatively small regions of the aperture?

Figures 13, 14, 15 and 16 are directed to question (1) above. These are photographs of the interference pattern in the monitor using Mirror #1 as the primary mirror in the telescope. Except for the shadow cast by the lens mount in the holographic setup (see Figures 5 & 6), the zone pattern on Mirror #1 covered the full 12" aperture. The diffraction efficiency of this pattern was .024% (see Section 7). From these results there appears little doubt but that acceptable fringe quality can be attained at diffraction efficiencies well below .01%. Signal intensities at a diffraction efficiency of .01% are entirely adequate for monitoring purposes (see Section 13.1).

Figure 17 is directed to question (2) above. This is a photograph of the interference pattern in the monitor using Mirror #2 as the primary mirror of the telescope. The step height of the zones was 5.0 nm on Mirror #2 (vs. 8.4 nm on Mirror #1). It was intended that the zones (and hence the fringe pattern) be suppressed on Mirror #2 in all areas except the annular and radial strips, each 1/4" wide, which appear in Figure 17. As discussed

INTERFEROMETER & SIMULATED STAR

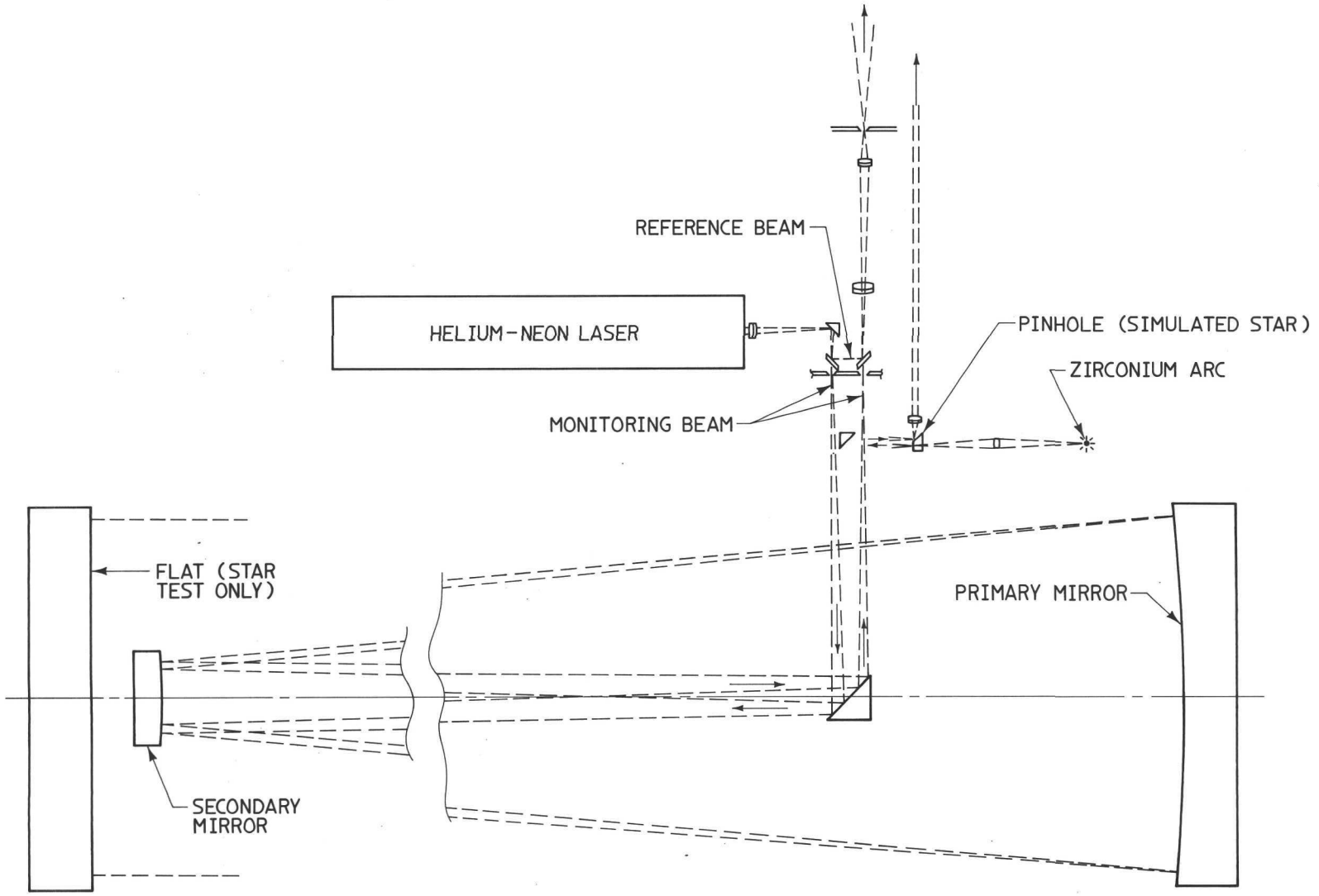

FIGURE 10

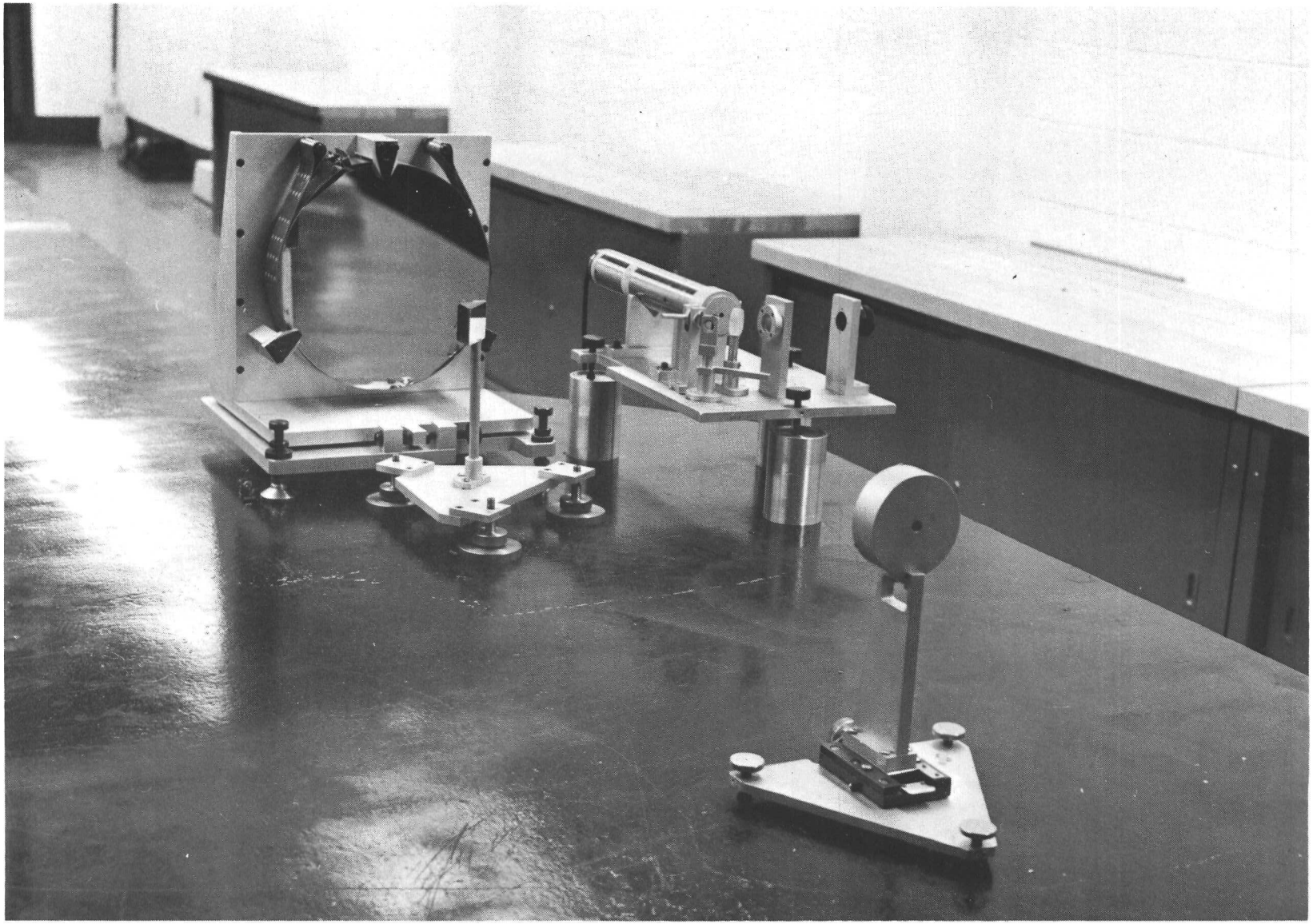

11. TELESCOPE AND INTERFEROMETER

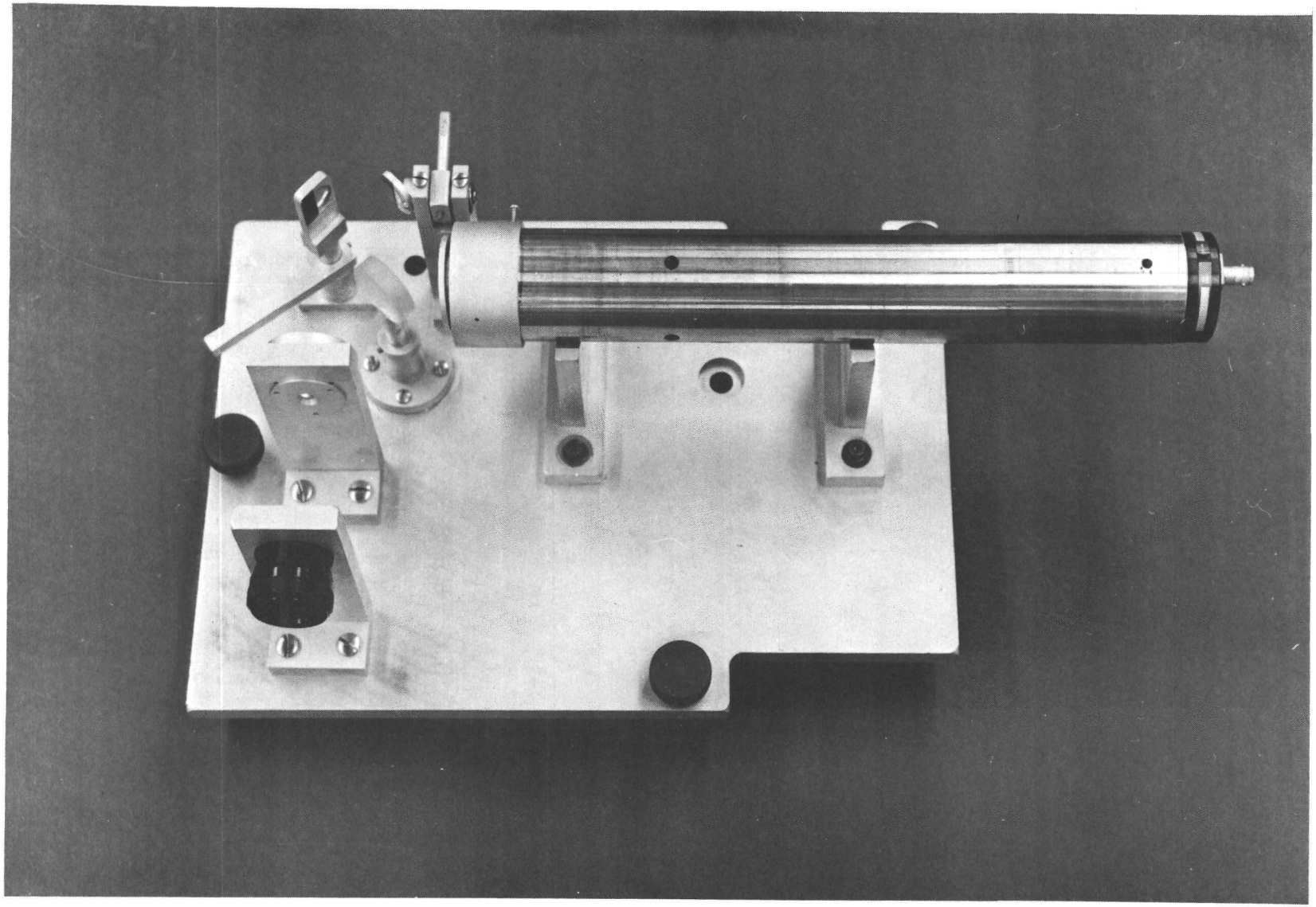

12. INTERFEROMETER

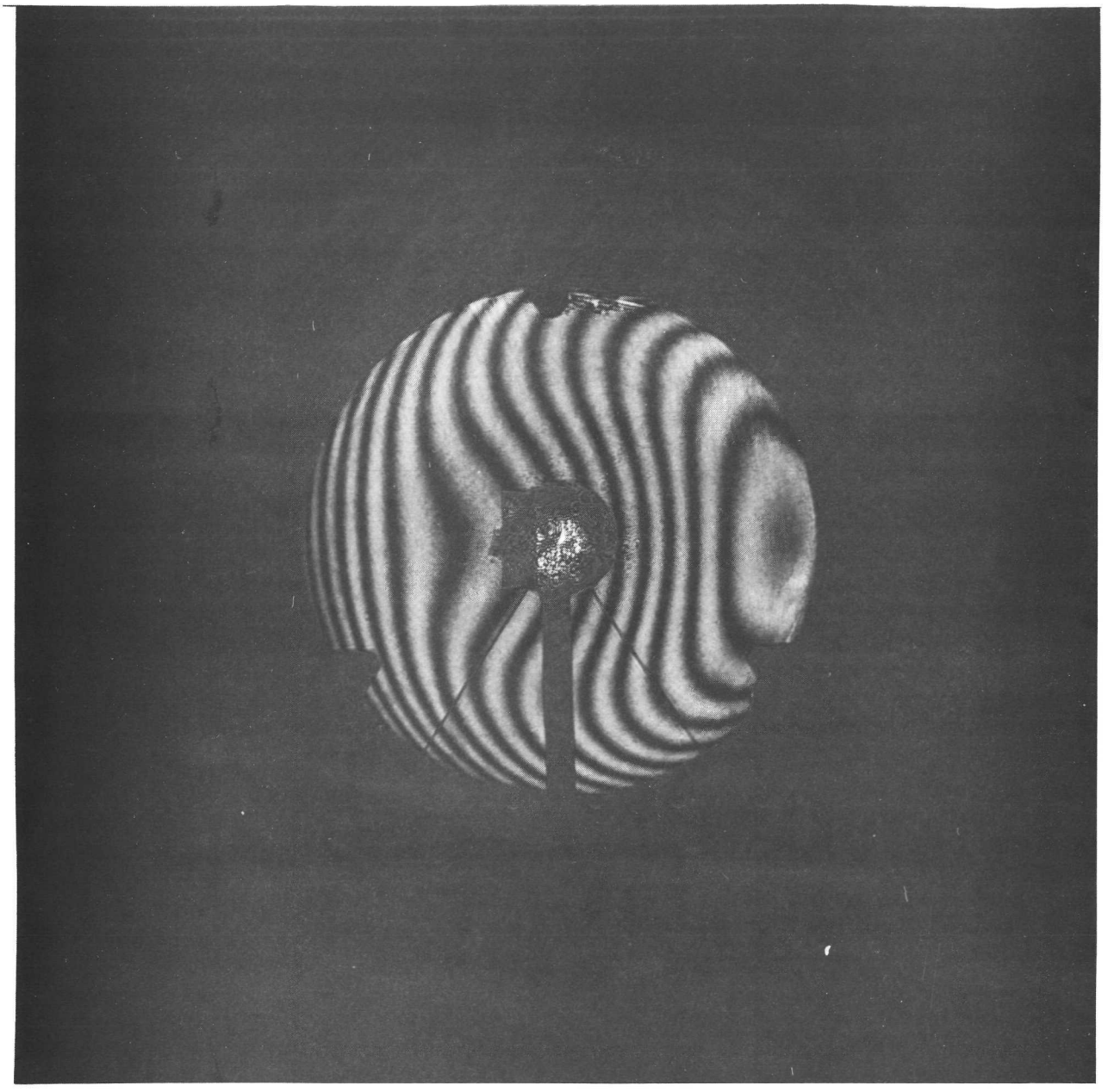

13. HORIZONTAL TILT

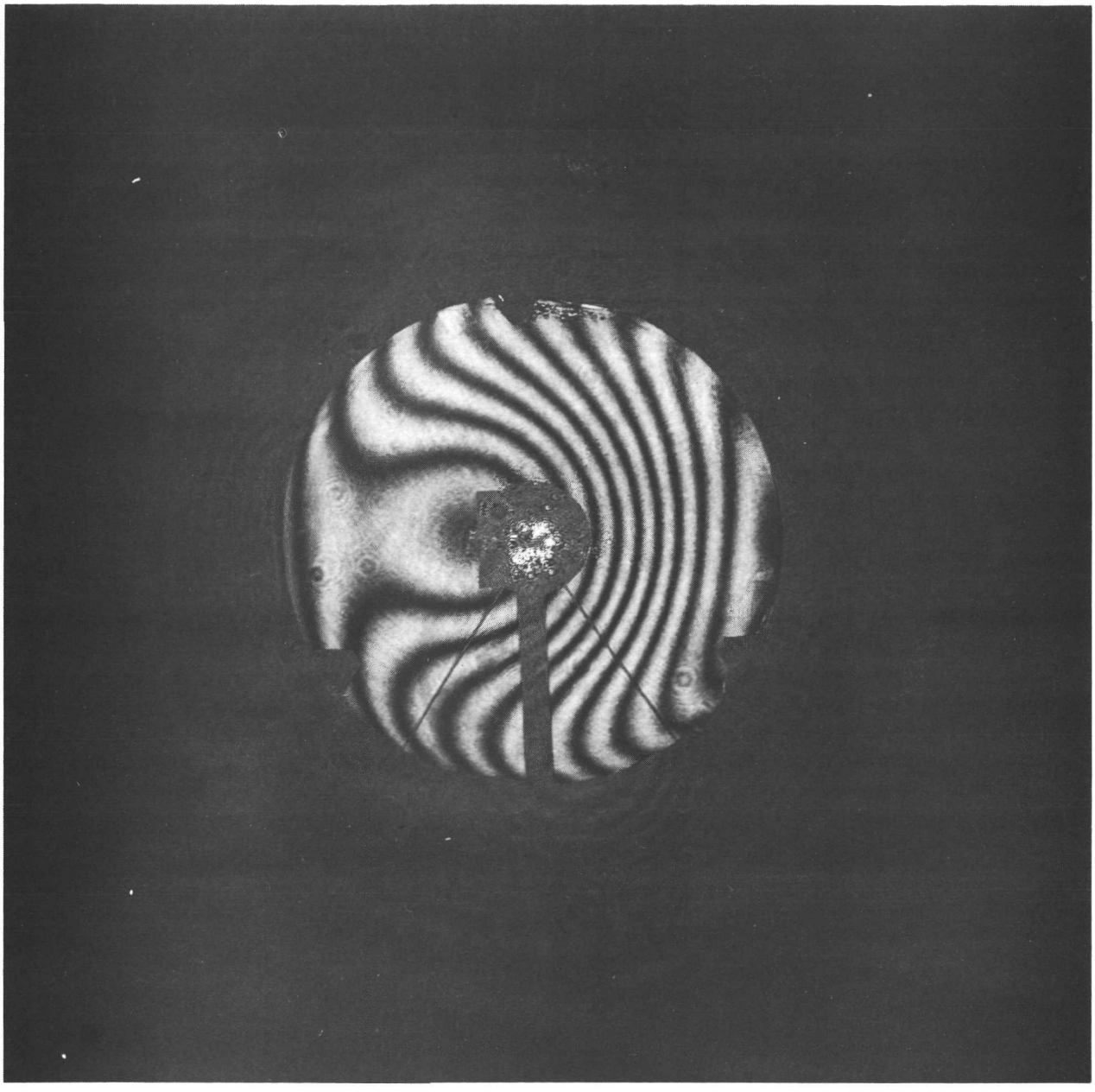

14. HORIZONTAL TILT AND DEFOCUSING INWARD

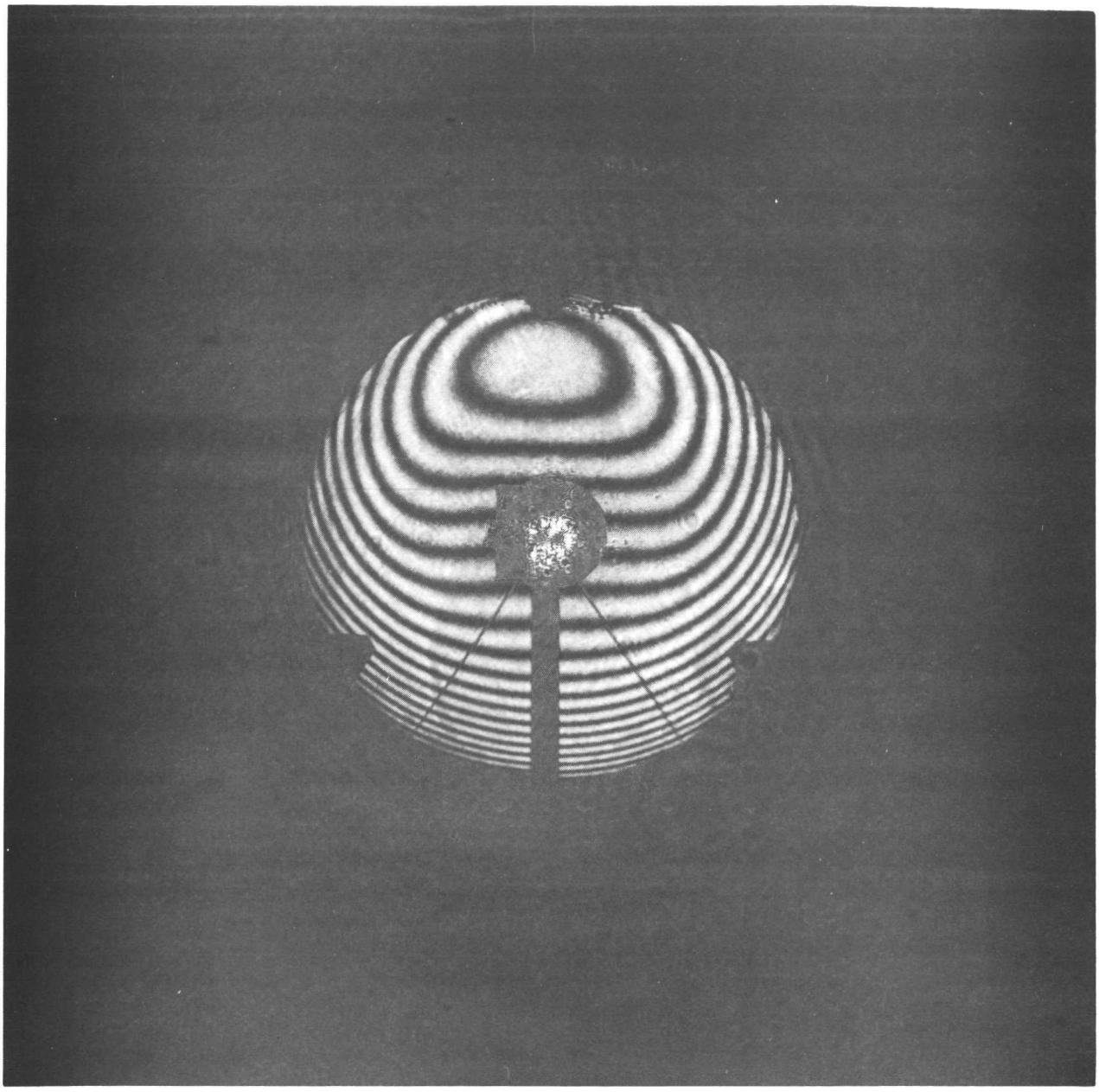

15. VERTICAL TILT AND DEFOCUSING OUTWARD

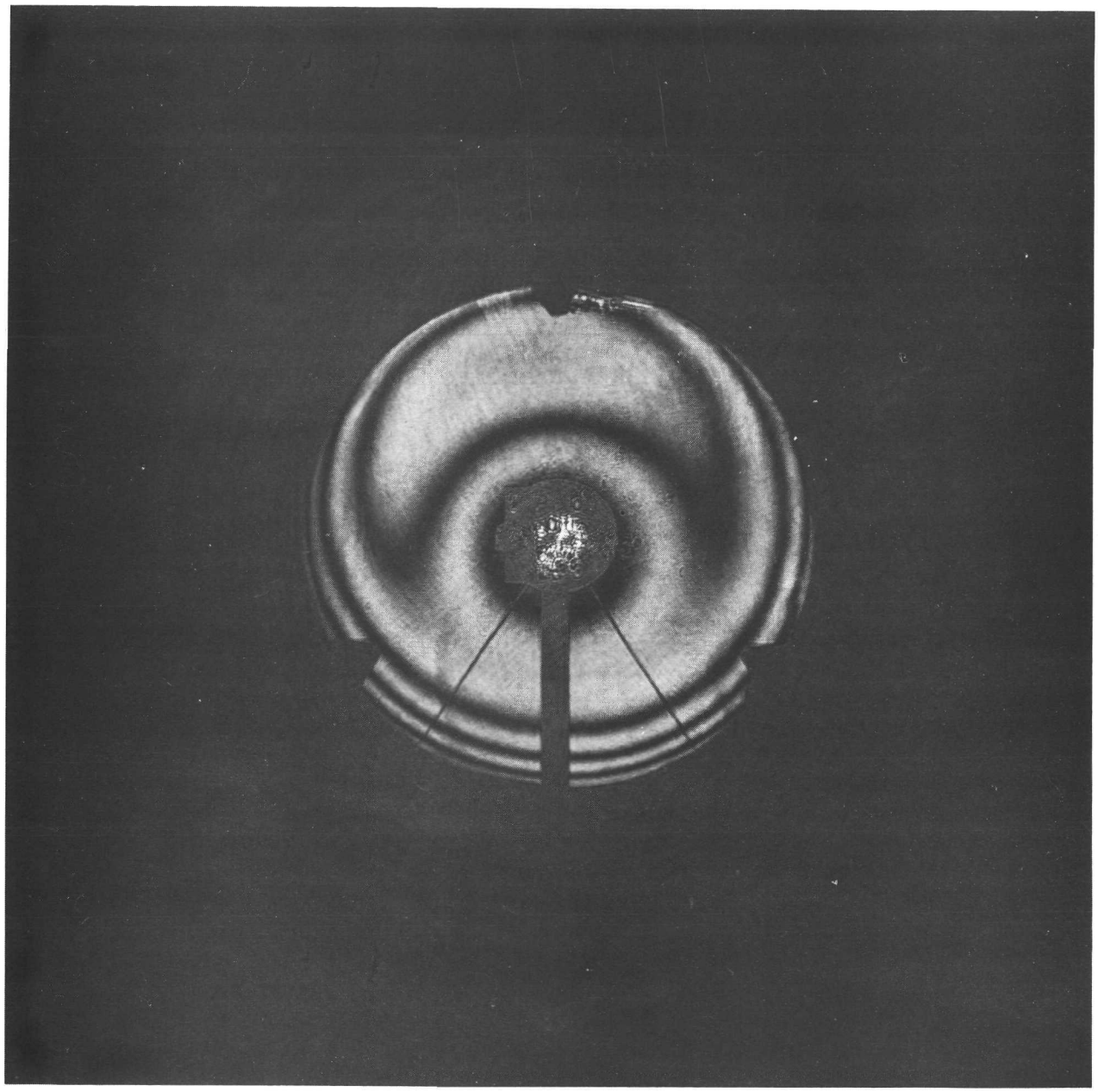

16. OPTIMUM FOCUS

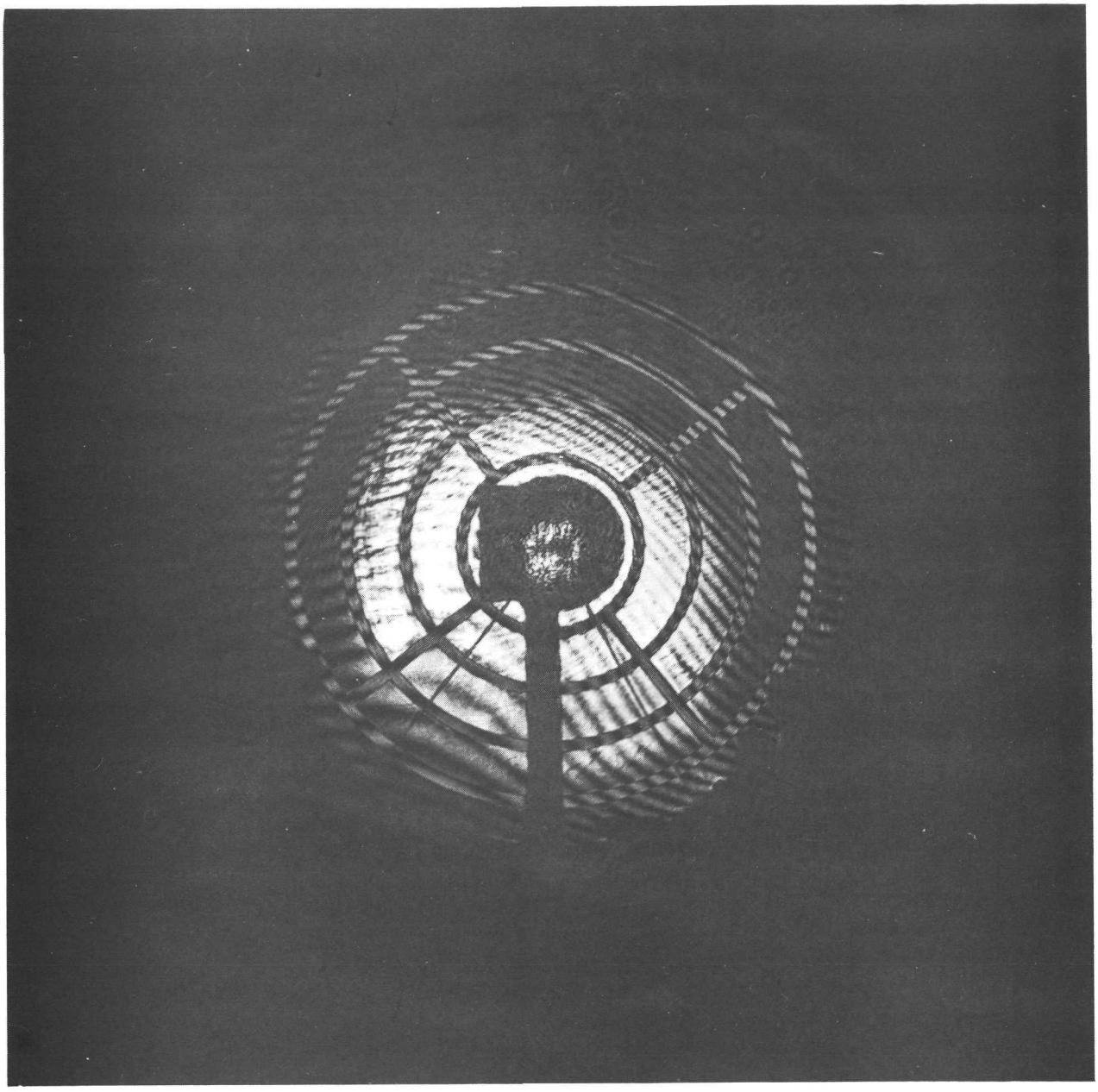

17. MASKED PATTERN

in Section 5.3.7, the photoresist could not be removed in the areas of intended suppression. This produced very strong diffraction in some areas, particularly toward the center, where none was intended. Figure 17 suffices, however, to show that distinct fringes can be readily discerned within relatively restricted regions of the mirror and that fringe continuity can be established via narrow strips connecting two points on the same fringe.

It should be noted in this context that fringe continuity can be established between isolated regions provided the figure of the mirror is stable enough that uncertainties do not exceed ± 1/2 fringe. An array of small isolated areas may therefore prove more useful than a pattern of interconnected areas.

Whatever the configuration of the zone pattern, it seems reasonable to expect that it may be restricted to less than 10% of the area. This reduces all the effects on stellar images by the equivalent of at least 2.5 stellar magnitudes. For a restricted pattern, Relation (20b) thus becomes:

$$M' > 32.5 \text{ magnitudes} \qquad (21)$$

9.0 STAR TEST

A star test was performed to determine if the zone pattern on the primary mirror has any observable effect upon the quality of stellar images. The test arrangement is shown in Figure 10.

The source was a pinhole illuminated by a zirconium arc. This pinhole subtended approximately 1/5th the diameter of the diffraction disc of the imaging optics. The telescope was double-passed via a flat mirror. All optical surfaces were regular to $\lambda_o/10$ or better.

Test results are shown in Figures 18 and 19. The results in Figure 18 are for a mirror with no zone pattern and the results in Figure 19 are for a mirror imprinted with a zone pattern covering the entire aperture of the mirror. This zone pattern was etched through a copper layer 5.0 nm thick.

The regularity of the substrate was somewhat less perfect in the case of the mirror bearing the zone pattern. Nevertheless the differences do not appear significant nor is there any reason theoretically to expect that there should be any significant difference arising from the zone pattern. Both images exhibit a crescent-shaped flare which is due to diffraction from the mount that holds the Newtonian folding mirror.

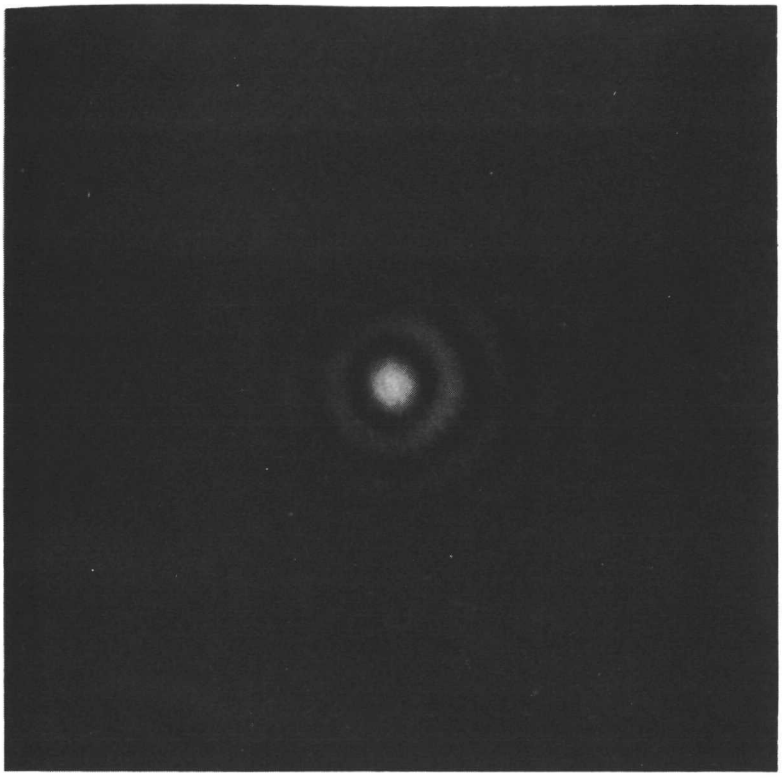

18. STAR TEST (NO ZONE PATTERN)

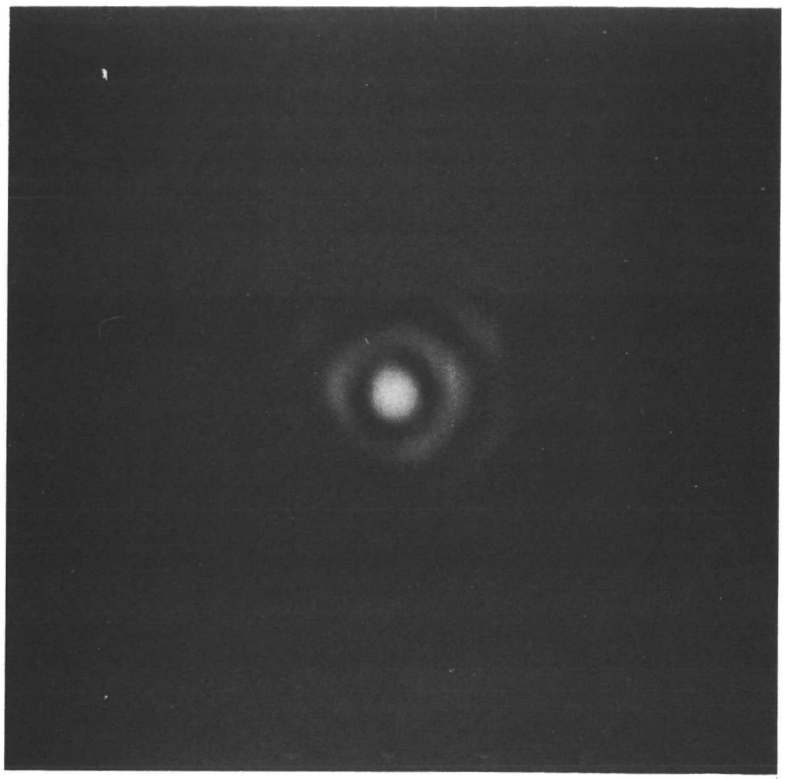

19. STAR TEST (WITH ZONE PATTERN)

10.0 SCATTER TESTS

10.1 Procedure

Figure 9 shows the arrangement for the scatter tests. An argon laser emitting .300 watts at λ = 488 nm served as the simulated stellar source. Baffeling was provided to minimize the effect of light scattered from surfaces other than the mirror.

A scatter test was made at a small angle (0^{o} 10') and also at a larger angle (1.1^{o}). For each test an exposure was made of the scattered light and a reference exposure was made of the stellar image. During the reference exposure, the illuminance of the stellar image was reduced to give a photographic density equal to that obtained for the scattered light. This reduction in illuminance was accomplished by two means:
(a) A calibrated filter was inserted into the beam.
(b) The exposed area was increased by defocussing the stellar image.
The ratio between the illuminance I_s of the scattered light and the average illuminance I_o within the Airy disc was computed from the following relation:

$$\frac{I_s}{I_o} = \left(\frac{2.44\, f\lambda}{d}\right)^2 \left(\frac{T_o}{T}\right) \tau \qquad (22)$$

where:

I_s = Illuminance of the scattered light

I_o = Average illuminance within the Airy disc

d = Diameter of the defocussed stellar image

f = Focal ratio of the mirror

λ = Wavelength of the simulated starlight

τ = Transmission factor of the attenuator

T = Duration of the exposure to scattered light

T_o = Duration of the exposure to the defocussed stellar image

I_s/I_o may be expressed in terms of stellar magnitudes by the following relation:

$$m_s - m_o = 2.5 \log\left(\frac{I_o}{I_s}\right) \qquad (23)$$

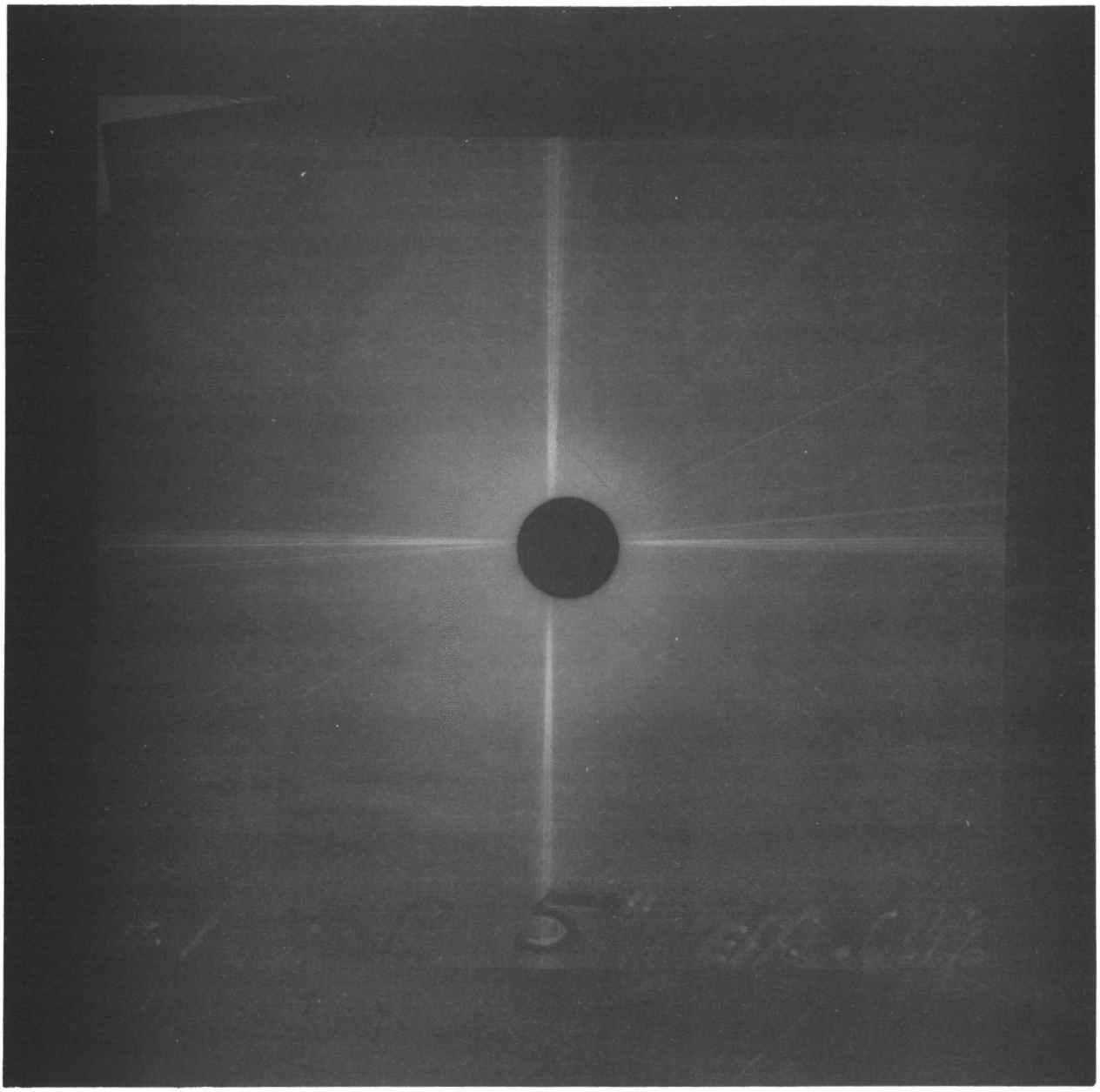

20. SMALL ANGLE SCATTER

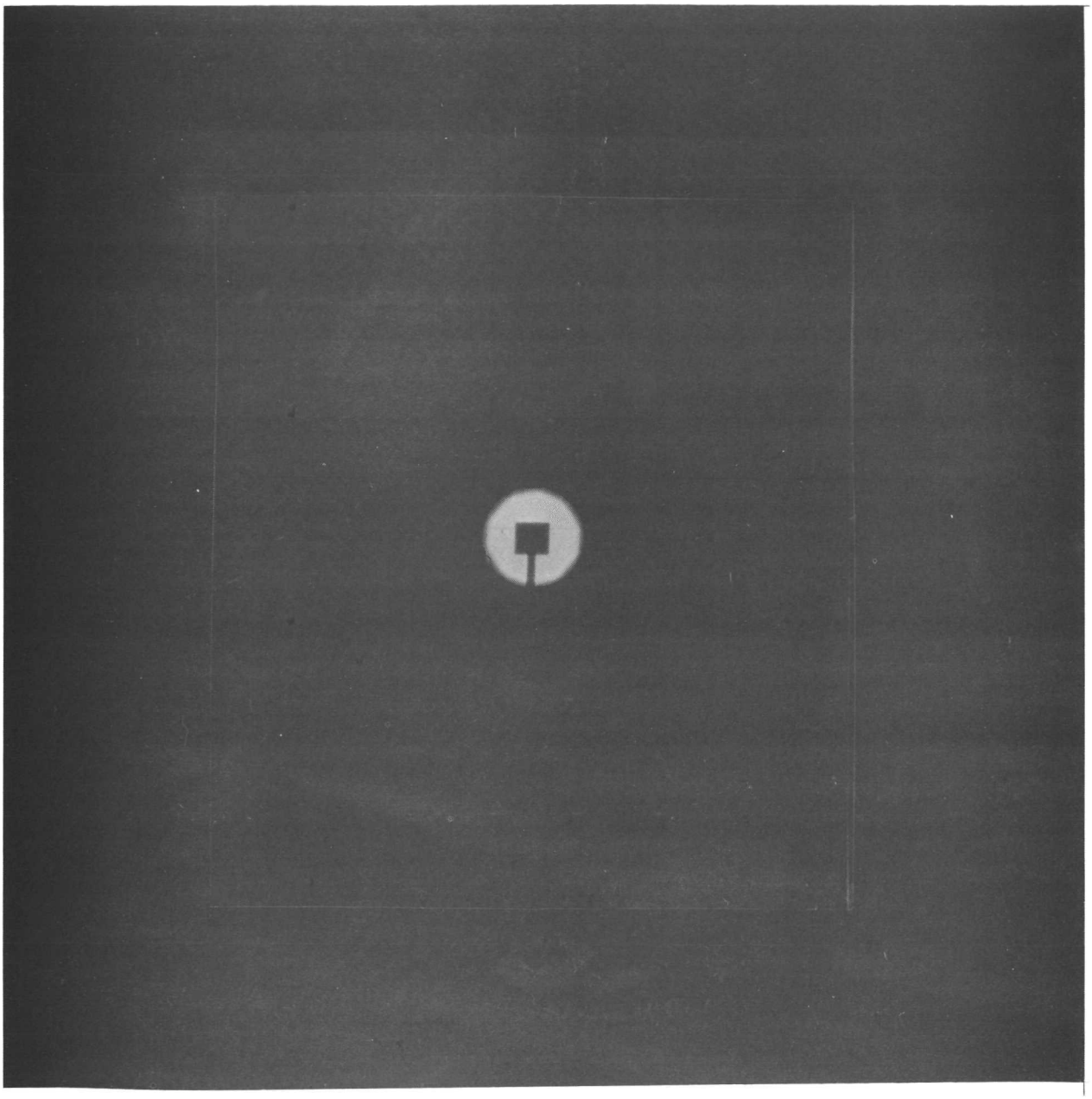

21. DEFOCUSED STELLAR IMAGE

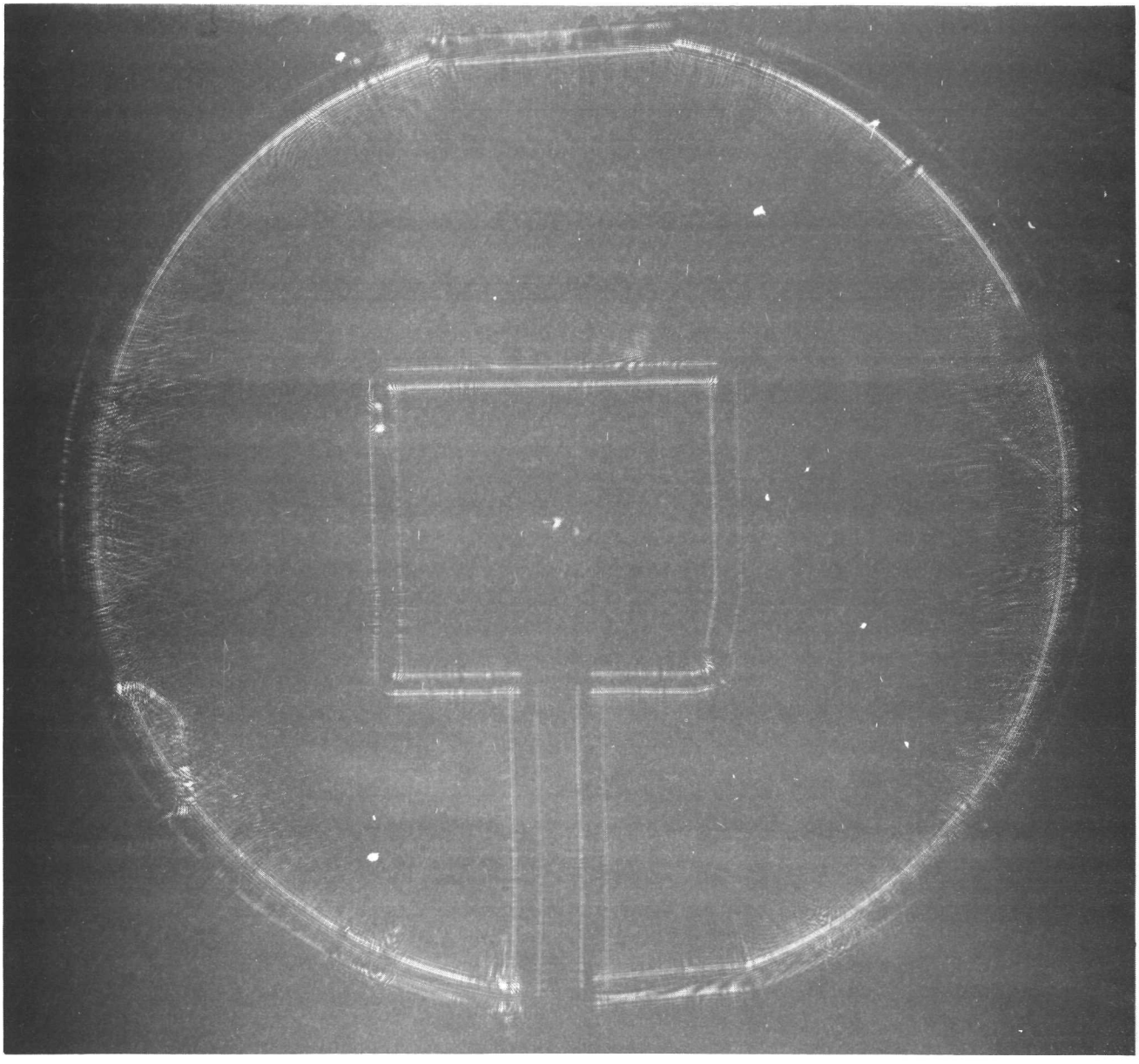

22. SCHLIEREN PHOTOGRAPH OF FILM HOLDER

where:

m_o = Magnitude of the zero order image

m_s = Magnitude of the light scattered into an area equal to that of the Airy diffraction disc.

10.2 Results

Figures 20 and 21 show a pair of exposures. Figure 20 is an exposure to small angle scattering and Figure 21 is an exposure to the defocussed stellar image. The shadow of the film holder appears in the defocussed stellar image.

In the exposures to scattered light, a 6 mm diameter hole in the film (see Figure 20) allowed the stellar image to pass through unobstructed as illustrated in Figure 9. At small scattering angles diffracted light was not present, the film being located within the diffracted shadow of the film holder. The relatively strong vertical and horizontal streaks in Figure 20 are due to residual diffraction and scatter from the film holder. A schlieren photograph of this diffraction and scatter appears in Figure 22. The fainter diagonal streaks in Figure 20 are from scratches on the mirror. These streaks were avoided in making density measurements.

For small angle scattering the density measurement was taken at a point 4.5 mm off axis which corresponds to a scattering angle of 0° 10'. At this position the value of $m_s - m_o$ computed from Relations (22) and (23) was:

$$m_s - m_o = 25.4 \text{ magnitudes} \qquad (24)$$

The values used in this computation were:

f = 5

λ = 488 nm

d = 6.0 mm

τ = .0021%

T = 5 sec

T_o = 15 sec

The measurement of large angle scatter was made in a manner similar to the measurement of small angle scatter, but in this case it was necessary to block the first order diffracted light by placing a small stop at the first order focus (see Figure 9). The measurement was made at a point where the intensity of the scattered light had dropped to 0.1% of the value obtained for the small angle measurement. This occurred at a point approximately 30 mm off-axis which corresponds to a scattering angle of 1.1°. At this position the value of $m_s - m_o$ computed from Relations (22) and (23) was:

$$m_s - m_o = 32.9 \text{ magnitudes} \tag{25}$$

10.3 Discussion

Comparison of (18) with (25) shows that the intensity of the scattered light rose above the intensity of the diffracted light for scattering angles less than about 1°. The large amount of small angle scatter was due principally to photographic debris on the mirror. Repeated stripping of the chrome undercoat during previous trials no doubt contributed to the scatter as did scratches which occurred during removal of the photoresist.

In contrast with scratches and photographic debris, the spatial frequencies of the zones themselves, are very high. Scattering due to zonal irregularities therefore occurs principally at relatively large angles. For angles greater than about 1°, the intensity of the scattered light rapidly fell far below that of the diffracted light. It thus appears that scattering from the zones themselves will not be the limiting factor. The zone generating process, however, must be relatively free of debris.

If, as seems probable, zones can be generated by some process which is relatively free of debris, it appears reasonable to expect that a zone pattern restricted both in area and in diffraction efficiency can approach the performance predicted by Relation (21). If this is true, there should be reasonable contrast between stellar images and background due to the zone pattern for stars brighter than about magnitude 29.

11.0 CONCLUSIONS

There is no indication that a zone pattern on the primary mirror will have any adverse affect on the quality of the stellar images.

Provided the zone generating process is reasonably free of debris, diffraction from the zones will probably dominate over scatter arising from the zones.

A first order diffraction efficiency of $\epsilon_1 < .01\%$ will suffice for monitoring purposes. This corresponds to an effective relief height (at $\lambda_o = 633$ nm) of $t' < 1.6$ nm.

In the spectral region above 100 nm, the intensity of stellar light diffracted from a zone pattern covering the full aperture of a 3 m telescope can probably be kept below that of the Airy disc of a star of magnitude 30.

The zone pattern may be restricted to small regions of the primary mirror and yet be useful for monitoring purposes.

If restricted to minimal area and to minimal diffraction efficiency, a usable zone pattern will probably not significantly affect the normal operation of a 3 m telescope in the spectral region above 100 nm for stars brighter than magnitude 29.

12.0 ACKNOWLEDGEMENT

The experimental work was handled by Mr. Roland Francois whose skill and diligence resulted in a near-perfect zone pattern over a full 12" aperture.

13.0 APPENDIX

13.1 Signal Power at the Sensors

In a heterodyne detection system, the signal power, P_s, incident on a single sensor is:

$$P_s = 2\gamma_1\sqrt{P_r P_m} \tag{26}$$

where:

γ_1 = Fraction of the total mirror area imaged onto a single sensor.

P_r = Power in the reference beam.

P_m = Power in the monitoring beam.

We define:

τ_1, τ_2 = Transmissivity of the beamsplitters.

P_o = Power emitted by the laser.

γ_2 = Loss factor from stops, etc.

Thus:

$$P_r = \gamma_2 \tau_1 \tau_2 P_o$$
$$P_m = \gamma_2 (1-\tau_1)(1-\tau_2) \epsilon_N P_o \quad (27)$$

Substitution of (27) into (26) gives:

$$P_s = 2 \gamma_1 \gamma_2 P_o \sqrt{\tau_1 (1-\tau_1) \tau_2 (1-\tau_2) \epsilon_N} \quad (28)$$

The values of τ_1 & τ_2 which maximize P_s are:

$$\tau_1 = \tau_2 = 1/2 \quad (29)$$

Thus:

$$P_s = \frac{1}{2} \gamma_1 \gamma_2 P_o \sqrt{\epsilon_N} \quad (30)$$

If, for example, we take

$P_o = 10^{-3}$ watt

$\gamma_1 = 10^{-3}$

$\gamma_2 = .2$

$\epsilon_N = .01\%$

then,

$$P_s = 10^{-9} \text{ watt} \quad (31)$$

Since the signal is at a fixed frequency and a narrow noise bandwidth (of the order of 1 Hz) is desirable, synchronous detection can be used to advantage. Silicon detectors should, therefore, suffice for phase measurements to ± .1 radian (i.e., ± $\lambda_o/125$ in terms of mirror deformation).

13.2 Diffraction Analysis

13.2.1 Type "A" Zones

We are interested in the relative amount of light diffracted into

DIFFRACTION FROM TYPE "A" ZONES

N'=0

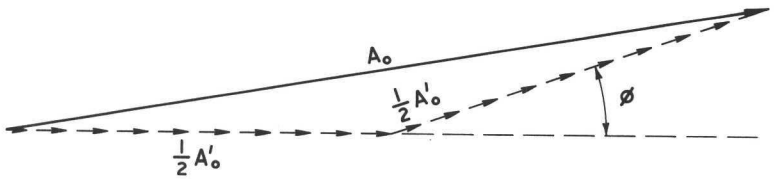

$$\phi = \frac{4\pi t}{\lambda}$$

$$A_0 = A'_0 \cos\frac{\phi}{2}$$

$$\epsilon_\lambda = 1 - \left(\frac{A_0}{A'_0}\right)^2 = \sin^2\frac{\phi}{2}$$

(a)

N'=1

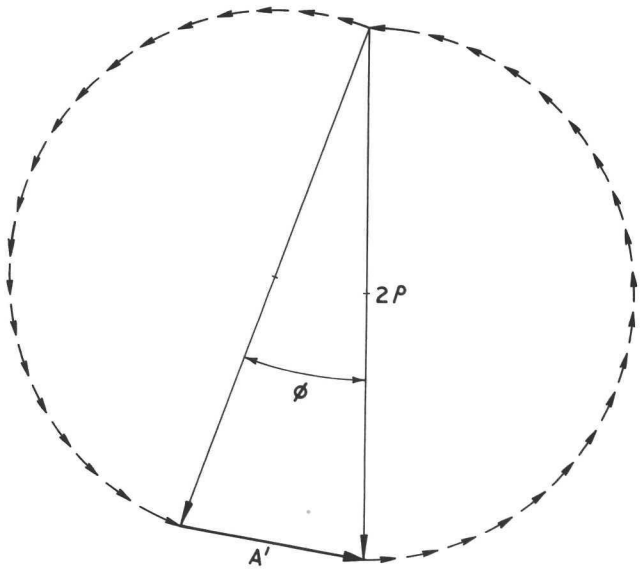

$$\phi = \frac{4\pi t}{\lambda}$$

$$A'_0 = 2\pi P$$

$$A_1 = 4\pi \sin\frac{\phi}{2}$$

$$\epsilon_1 = \left(\frac{A_1}{A'_0}\right)^2 = \left[\frac{2}{\pi}\sin\frac{\phi}{2}\right]^2$$

(b)

FIGURE 23

orders N = 0 and N = 1. The angular dependence is practically identical for orders N = 0 and N = 1. Therefore, for all practical purposes we may simply compare the peak intensities of orders N = 0 and N = 1.

We let:

I_o' = Peak intensity for order N = 0, assuming the zones to be absent.

I_o = Peak intensity for order N = 0 (when the zones are present).

I_1 = Peak intensity for order N = 1.

We also define the following:

λ = Wavelength of starlight

λ_o = Wavelength of the monitoring light

N = Order of diffraction

τ = Step height

ϵ_λ = Diffraction efficiency for all orders combined (except N = 0), at wavelength λ.

ϵ_1 = Diffraction efficiency for order N = 1 at wavelength λ_o.

We also define the following field amplitudes:

$$A_o' = \sqrt{I_o'}$$

$$A_o = \sqrt{I_o} \qquad (32)$$

$$A_1 = \sqrt{I_1}$$

Hence:

$$\epsilon_\lambda = \frac{I_o' - I_o}{I_o'} = 1 - \left(\frac{A_o}{A_o'}\right)^2$$

$$\epsilon_1 = \frac{I_1}{I_0'} = \left(\frac{A_1}{A_0'}\right)^2 \quad [@\ \lambda = \lambda_0] \tag{34}$$

Neglecting very small obliquity effects, the integration of any component of the field amplitude over one complete zone period may be represented graphically in the complex plane as shown in Figure 23a (for N = 0) and in Figure 23b (for N = 1). The net contributions from successive zones are all in phase; integration over a single zone therefore suffices to give the proper ratios for N = 0 and N = 1.

As far as ratios are concerned, the integrated curve length (short arrows) may be considered as representing A'_0. The resultant vector then represents A_0 in Figure 23a and A_1 in Figure 23b.

For order N = 0, the phase is constant over each half-zone. There is a phase jump of $\phi = \frac{4\pi t}{\lambda}$ due to the step height, t, between the half zones. From Figure 23a it follows that:

$$A_0 = A_0' \cos\frac{\phi}{2} \tag{35}$$

Substitution of (35) into (33) gives:

$$\epsilon_\lambda \approx \sin^2\frac{\phi}{2} \tag{36}$$

Where:

$$\phi = \frac{4\pi t}{\lambda} \tag{37}$$

For order N = 1, the phase varies uniformly through half a cycle over each half-zone. There is again a phase jump of ϕ due to the step height, t, between the two half-zones. From Figure 23b it follows that:

$$A_0' = 2\pi\rho$$

$$A_1 = 4\pi \sin\frac{\phi}{2} \tag{38}$$

Substitution of (38) into (34) gives:

$$\epsilon_1 = \left[\frac{2}{\pi} \sin \frac{\phi}{2}\right]^2 \tag{39}$$

where,

$$\phi = \frac{4\pi t}{\lambda_o} \tag{40}$$

Since $\phi << \frac{\pi}{2}$, the following approximation for (39) is valid:

$$\epsilon_1 \approx \left(\frac{4t}{\lambda_o}\right)^2 \tag{41}$$

Comparison of (36) with (39) shows that:

$$\epsilon_\lambda = \left(\frac{\pi}{2}\right)^2 \epsilon_1 \qquad [@\ \lambda = \lambda_o] \tag{42}$$

13.2.2 Type "B" Zones

As for type "A" zones, we are interested only in ratios. Since $a >> N\lambda_o$ (where a = zone period), the angular dependence is practically the same for all orders $N' \leq N$. Therefore, as in Section 13.2.1, we simply compare the peak intensities of the various orders.

We define:

$I_{N'}$ = Peak intensity for order N'.

$\epsilon_{N'}$ = Diffraction efficiency for order N' at wavelength λ.

$A_{N'} = \sqrt{I_{N'}}$

$2Nb$ = Full zone period

ηb = Width of the narrower subzone } (see Figure 3)

As in the case of type "A" zones, we have:

$$\epsilon_\lambda = \frac{I_o' - I_o}{I_o'} = 1 - \left(\frac{A_o}{A_o'}\right)^2 \tag{43}$$

DIFFRACTION FROM TYPE "B" ZONES

$N'=0$

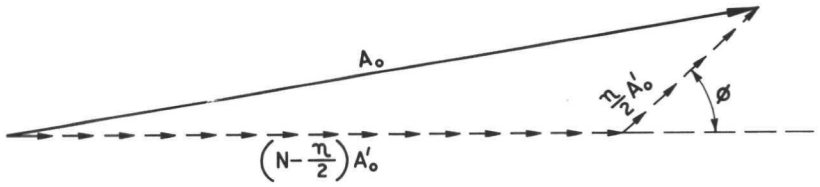

$$\phi=\frac{4\pi t}{\lambda}=\frac{\pi\lambda_o}{\lambda}$$

$$A_o^2=\left[\left(N-\frac{\eta}{2}\right)A'_o\right]^2+\left[\frac{\eta}{2}A'_o\right]^2+\left(N-\frac{\eta}{2}\right)\eta\left(A'_o\right)^2\cos\phi$$

$$\epsilon_\lambda=1-\left(\frac{A_o}{A'_o}\right)^2=2\left(1-\frac{\eta}{2N}\right)\frac{\eta}{N}\sin^2\phi$$

(a)

$N'\neq 0$

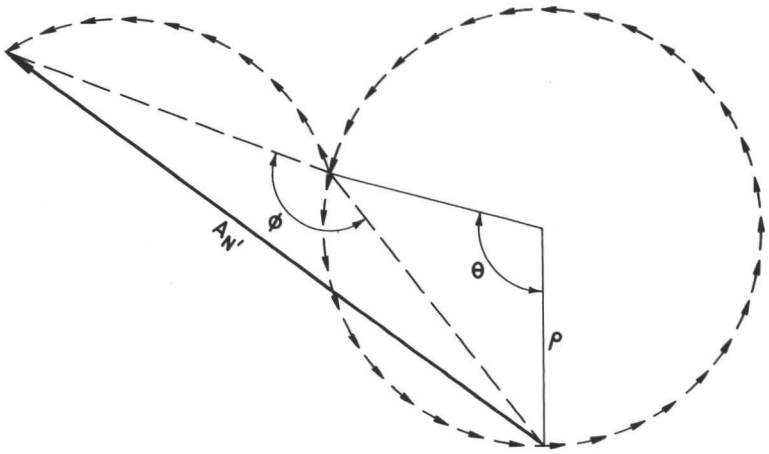

$$\theta=\pi\eta\frac{N'}{N}$$

$$\phi=\frac{4\pi t}{\lambda}=\frac{\pi\lambda_o}{\lambda}$$

$$A'_o=2\pi\rho N'$$

$$A_{N'}=4\rho\sin\frac{\theta}{2}\sin\frac{\phi}{2}$$

$$\epsilon_{N'}=\left(\frac{A_{N'}}{A'_o}\right)^2=\left[\frac{2}{\pi N'}\sin\frac{\theta}{2}\sin\frac{\phi}{2}\right]^2$$

(b)

FIGURE 24

$$\epsilon_{N'} = \frac{I_{N'}}{I_0'} = \left(\frac{A_{N'}}{A_0'}\right)^2 \tag{44}$$

The amplitude integrals are shown schematically in Figures 24a and 24b.

For order N' =0 (see Figure 24a), the phase is constant over both the narrower and the wider regions. There is a phase jump $\phi = \frac{\pi \lambda_0}{\lambda}$ due to the step height, $\frac{\lambda_0}{4}$, between the two regions.

From Figure 24a, it follows from the cosine law that:

$$A_0^2 = \left[\left(1-\frac{\eta}{2N}\right)A_0'\right]^2 + \left[\frac{\eta}{2N}A_0'\right]^2 - \left(1-\frac{\eta}{2N}\right)\frac{\eta}{N}(A_0')^2 \cos\phi \tag{45}$$

Substitution of (45) into (43) gives:

$$\epsilon_\lambda = 2\left(1-\frac{\eta}{2N}\right)\frac{\eta}{N}\sin^2\frac{\phi}{2} \tag{46}$$

Where:

$$\phi = \frac{4\pi t}{\lambda} = \frac{\pi \lambda_0}{\lambda} \tag{47}$$

For order N' $\neq$ 0 (see Figure 24b), the phase varies continuously through $\frac{\eta N'}{2N}$ cycles over the narrower region.

There is a phase jump of $\phi = \frac{\pi \lambda_0}{\lambda}$ due to the step height, $\frac{\lambda_0}{4}$, between the two regions.

From Figure 24b it follows that:

$$\begin{aligned} A_0' &= 2N'\pi P \\ A_{N'} &= 4P \sin\frac{\theta}{2}\sin\frac{\phi}{2} \end{aligned} \tag{48}$$

Substitution of (48) into (44) gives:

$$\epsilon_{N'} = \left[\frac{2}{\pi N'}\sin\frac{\theta}{2}\sin\frac{\phi}{2}\right]^2 \tag{49}$$

Where:

$$\theta = \pi \eta \frac{N'}{N} \tag{50}$$

$$\phi = \frac{4\pi t}{\lambda} = \frac{\pi \lambda_0}{\lambda} \tag{51}$$

For order N' = N, this reduces to:

$$\epsilon_N = \left[\frac{2}{\pi N} \sin\left(\frac{\eta \pi}{2}\right) \right]^2 \tag{52}$$

13.3 Holographic Parameters

The basic geometrical relationships are given in Figure 25. Parameters α and β are to be chosen so as to minimize the aberration M. In the remainder of this section it will be shown that this results in the following formulae for α and β :

$$\alpha = \frac{4\gamma^2 - \gamma - 2 + \sqrt{4 - 3\gamma^2}}{2\gamma(1-\gamma)} \tag{a}$$

$$\beta = \frac{4\gamma^2 + \gamma - 2 + \sqrt{4 - 3\gamma^2}}{2\gamma(1+\gamma)} \tag{b}$$

(53)

Where:

$$\gamma = \frac{\lambda'}{\lambda_0} \tag{c}$$

For the ideal geometry, the interference pattern on the mirror consists of circular fringes formed by interference between a plane wave and a wave diverging from focal point 0 . The fringe number (counted from the center) is given by:

$$M_0 = \frac{1}{\lambda_0}(a - b) \tag{54}$$

For the compromise geometry, the interference pattern consists of circular fringes formed by interference between a wave diverging from point P and a second wave diverging from point Q. The fringe number (counted from the center) is given by:

$$M = \frac{1}{\lambda'}(\alpha F + \beta F + c - d) \tag{55}$$

The difference in fringe number represents the aberration arising from the compromise geometry:

ZONE GEOMETRY

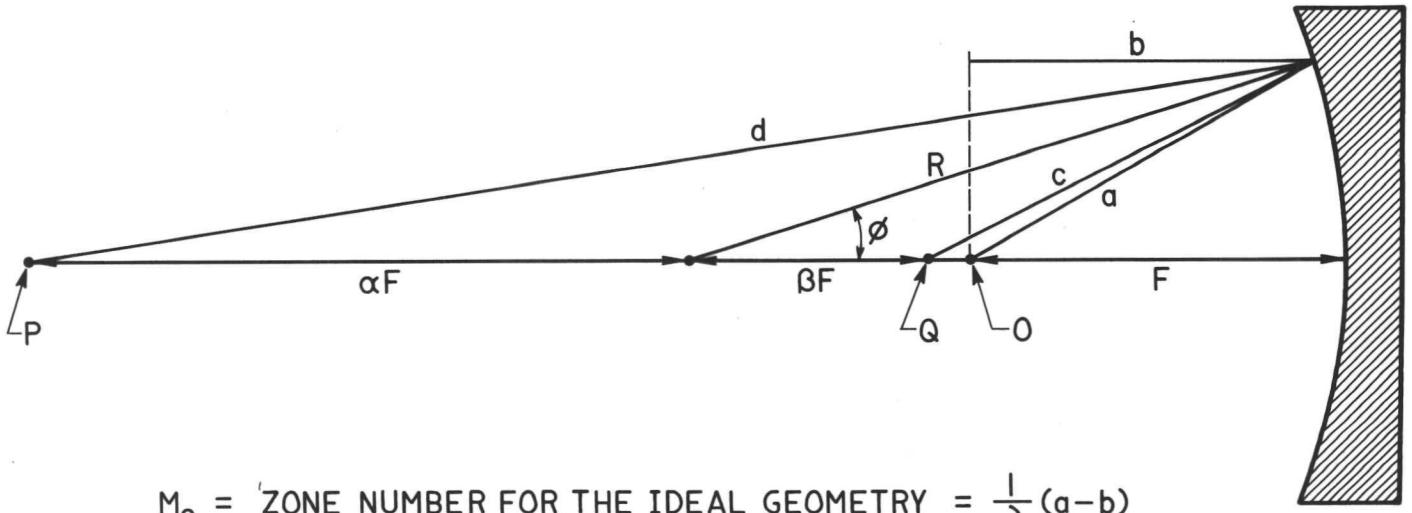

M_0 = ZONE NUMBER FOR THE IDEAL GEOMETRY = $\frac{1}{\lambda_0}(a-b)$

M = ZONE NUMBER FOR THE COMPROMISE GEOMETRY = $\frac{1}{\lambda'}(\alpha F + \beta F + c - d)$

2F = RADIUS OF THE BEST FITTING SPHERE

$$a^2 = R^2 + F^2 - 2RF\cos\phi$$

$$b = R\cos\phi - F$$

$$c^2 = R^2 + (\beta F)^2 - 2R(\beta F)\cos\phi$$

$$d^2 = R^2 + (\alpha F)^2 + 2R(\alpha F)\cos\phi$$

ZONE ABERRATION: $M_0 - M = \frac{1}{\lambda_0}(a-b) - \frac{1}{\lambda'}(\alpha F + \beta F + c - d)$

FIGURE 25

$$\Delta M = \frac{1}{\lambda_0}(a-b) - \frac{1}{\lambda'}(\alpha F + \beta F + c - d) \tag{56}$$

Application of the Cosine Law to Figure 25 gives the following relations:

$$\begin{aligned} a^2 &= R^2 + F^2 - 2RF\cos\phi \\ b &= R\cos\phi - F \\ c^2 &= R^2 + (\beta F)^2 - 2R\beta F\cos\phi \\ d^2 &= R^2 + (\alpha F)^2 + 2R\alpha F\cos\phi \end{aligned} \tag{57}$$

We choose the best-fitting sphere of radius 2F and denote the interval between the mirror surface and this sphere by $2F\delta_0$:

$$2F\delta_0 = R - 2F \tag{58}$$

or:

$$R = 2F(1+\delta_0) \tag{59}$$

δ_0 is very small.

We also define:

$$\nu = 1 - \cos\phi \tag{60}$$

ν is also small but not as small as δ_0.

Combining (58) and (60) with (57) gives:

$$\begin{aligned} a^2 &= F^2[1 + 4\nu + 4\delta_0(1+\nu+\delta_0)] \\ b &= F[1 - 2\nu + 2\delta_0(1-\nu)] \\ c^2 &= F^2[(2-\beta)^2 + 4\beta\nu + 4\delta_0(2-\beta+\beta\nu+\delta_0)] \\ d^2 &= F^2[(2+\alpha)^2 - 4\alpha\nu + 4\delta_0(2+\alpha-\alpha\nu+\delta_0)] \end{aligned} \tag{61}$$

We define:

$$\begin{aligned}
\Delta_a &= 4\delta_0(1+v+\delta_0) \\
\Delta_b &= 2\delta_0(1-v) \\
\Delta_c &= 4\delta_0(2-B+Bv+\delta_0) \\
\Delta_d &= 4\delta_0(2+\alpha-\alpha v+\delta_0)
\end{aligned} \tag{62}$$

Using definitions (62) in (61) gives:

$$\begin{aligned}
a &= F[1+4v+\Delta_a]^{\frac{1}{2}} \\
b &= F[1-2v+\Delta_b] \\
c &= F[(2-B)^2+4Bv+\Delta_c]^{\frac{1}{2}} \\
d &= F[(2+\alpha)^2-4\alpha v+\Delta_d]^{\frac{1}{2}}
\end{aligned} \tag{63}$$

We use the binomial theorem to expand (63) up to terms of 1st order in δ_0 and 3rd order in v:

$$\begin{aligned}
a &= F\left[1+2v-2v^2+4v^3+\frac{\Delta_a}{2}-v\Delta_a\right] \\
b &= F[1-2v+\Delta_b] \\
c &= F\left[(2-B)+\frac{2Bv}{(2-B)}-\frac{2B^2v^2}{(2-B)^3}+\frac{4B^3v^3}{(2-B)^5}-\frac{Bv\Delta_c}{(2-B)^3}+\frac{\Delta_c}{2(2-B)}\right] \\
d &= F\left[(2+\alpha)-\frac{2\alpha v}{(2+\alpha)}-\frac{2\alpha^2v^2}{(2+\alpha)^3}-\frac{4\alpha^3v^3}{(2+\alpha)^5}+\frac{\alpha v\Delta_d}{(2+\alpha)^3}+\frac{\Delta_d}{2(2+\alpha)}\right]
\end{aligned} \tag{64}$$

Terms in δ_o and v^3 are very small. We therefore drop these and all higher terms from (64):

$$a = F[1 + 2v - 2v^2]$$

$$b = F[1 - 2v]$$

$$c = F\left[(2-\beta) + \frac{2\beta v}{(2-\beta)} - \frac{2\beta^2 v^2}{(2-\beta)^3}\right] \tag{65}$$

$$d = F\left[(2+\alpha) - \frac{2\alpha v}{(2+\alpha)} - \frac{2\alpha^2 v^2}{(2+\alpha)^3}\right]$$

Substitution of (65) into (56) (setting $\Delta M = 0$) gives:

$$\frac{1}{\lambda_o}[4v - 2v^2] = \frac{1}{\lambda'}\left[\frac{2\beta v}{(2-\beta)} + \frac{2\alpha v}{(2+\alpha)} - \frac{2\beta^2 v^2}{(2-\beta)^3} + \frac{2\alpha^2 v^2}{(2+\alpha)^3}\right] \tag{66}$$

Equating terms in v gives:

$$\frac{2}{\lambda_o} = \frac{1}{\lambda'}\left[\frac{\beta}{(2-\beta)} + \frac{\alpha}{(2+\alpha)}\right] \tag{67}$$

Equating terms in v^2 gives:

$$\frac{1}{\lambda_o} = \frac{1}{\lambda'}\left[\frac{\beta^2}{(2-\beta)^3} - \frac{\alpha^2}{(2+\alpha)^3}\right] \tag{68}$$

We make the following substitutions:

$$2 - g = \beta \tag{69}$$

$$h - 2 = \alpha \tag{70}$$

(67) and (68) thus become:

$$\frac{2}{\lambda_o} = \frac{1}{\lambda'}\left[\frac{(2-g)}{g} + \frac{(h-2)}{h}\right] \tag{71}$$

$$\frac{1}{\lambda_o} = \frac{1}{\lambda'}\left[\frac{(2-g)^2}{g^3} - \frac{(h-2)^2}{h^3}\right] \tag{72}$$

Cross multiplication of (71) with (72) gives:

$$2(2-g)^2h^3 - 2(h-2)^2g^3 = g^2h^3(2-g) + g^3h^2(h-2) \tag{73}$$

(73) reduces to:

$$(1-g)h^3 = (1-h)g^3 \tag{74}$$

Solving (71) for and gives:

$$g = \frac{h}{1+\gamma h} \tag{75}$$

$$h = \frac{g}{1-\gamma g} \tag{76}$$

where:

$$\gamma = \frac{\lambda'}{\lambda_0} \tag{77}$$

Substitution of (76) into (74) gives:

$$(1-g)g^3 = \left[(1-\gamma g)^3 - (1-\gamma g)^2 g\right] g^3 \tag{78}$$

$$(1-g) = 1 - 3\gamma g + 3\gamma^2 g^2 - \gamma^3 g^3 - g + 2\gamma g^2 - \gamma^2 g^3 \tag{79}$$

(79) reduces to:

$$\gamma(1+\gamma)g^2 - (2+3\gamma)g + 3 = 0 \tag{80}$$

The solution of (80) is:

$$g = \frac{2+3\gamma - \sqrt{4-3\gamma^2}}{2\gamma(1+\gamma)} \tag{81}$$

The sign of the radical in (81) is determined by the fact that

$g = 1$ when $\gamma = 1$.

Relations (75), (76) and (77) are invariant under the following transformation:

$$g \longrightarrow h \;;\; h \longrightarrow g \;;\; \gamma \longrightarrow -\gamma$$

Applying this transformation of (81) gives:

$$h = \frac{-(2-3\gamma) + \sqrt{4-3\gamma^2}}{2\gamma(1-\gamma)} \qquad (82)$$

Substitution of (69) into (81) and substitution of (70) into (82) proves (53).

An analysis of the magnitude of aberration ΔM [Relation (56)] may be found in Section 2.4.2.2 of Report NASA CR-111811.

13.4 General System Considerations

13.4.1 Monitoring and Controlling a Primary-Secondary System

In a completely general view, a holographic monitoring system contains a set of phase holograms most of which are restricted to small regions of the primary mirror but some of which may be located on the secondary mirror. From each hologram a phase signal ϕ_i is developed. The control system compares phases ϕ_i with a set of reference values ϕ'_i which correspond to optimum performance of the telescope. The control system then controls the focus, alignment and figure of the optics so as to maintain the condition $\phi_i = \phi'_i$.

In a closed loop control system, changes $d\phi_i$ in the stabilizing signals may be considered to be effectively linear functions of the actuator displacements dx_j, i.e., $d\phi_i = \sum_j A_{ij}\, dx_j$. The coefficients A_{ij} are derivable from design data and from observations of the system's actual responses. If there are more control actuators than there are stabilizing sensors, then the coefficients of the inverse relationship, $dx_i = \sum_j B_{ij}\, d\phi_j$, are indeterminate until further mathematical constraints are imposed. There is a great deal of freedom as to how these mathematical constraints are built into the computer program. If, on the other hand, there are more stabilizing sensors than there are control actuators, then the coefficients B_{ij} of the inverse relationship may be determined by a least-squares computation. This situation is considered less desirable because the calculation is less straight-forward and performance depends more critically upon an accurate knowledge of the coefficients B_{ij}.

The phase holograms on the primary mirror are illuminated via the secondary mirror. As long as the figure of the secondary mirror remains stable, this set of holograms provides information for stabilizing the focus of the telescopic system as well as information for stabilizing the figure of the primary mirror.

Alignment of the telescope involves four degrees of lateral freedom between the primary and secondary mirrors. The set of holograms on the primary mirror provides information for stabilizing two of these four degrees of lateral freedom. These two degrees of lateral freedom are the two most critical ones from the standpoint of image quality. The two less critical degrees of lateral freedom may be monitored in a similar manner using light diffracted from a set of phase holograms located around the periphery of the secondary mirror. Three such holograms (very faint) will suffice to provide the remaining stabilizing information for alignment of the telescope.

At the perimeter of the primary and secondary mirrors, there is probably no objection to using discrete reflectors rather than holograms imprinted on the mirror surface. One advantage of holograms, however, is that they may be continuous around the complete perimeter thus providing direct and unambiguous pictorial information by means of which alignment may be performed under operator control with the aid of a video monitor.

It should be noted that stabilization of the alignment of the telescope in the manner discussed above far exceeds the tolerance requirements imposed by image quality alone. Therefore, in the event that it should prove desirable to use the alignment controls for fine pointing, it is possible to allow the alignment stabilization to be overridden to some extent by the fine pointing control system. This has the disadvantage, however, that the optimum values ϕ'_i of the stabilizing signals are no longer fixed but must be continuously recalculated.

13.4.2 Calibration of the Holographic Monitor

Calibration of the holographic monitor consists of establishing the phase values ϕ'_i which correspond to optimum performance of the telescope.

There are two methods for determining the values ϕ'_i prior to launch:

(A) By use of an independent checkout system.
(B) By precise measurement of the geometry of the zone pattern.

Method (B) is considered to be the more practical. This is discussed in Section 1.5 and 2.2 of Report NASA CR-111811.

The values ϕ'_i can also be determined in orbit by means of an auxiliary checkout system which employs a stellar wavefront sensor. This is

considered to be the most accurate method. It has the further advantage that it can be repeated periodically to update the values ϕ'_i to eliminate possible errors due to gradual drift in the holographic monitor. In this case the holographic monitor may be viewed as a stabilizing system which stabilizes the optical performance of the telescope between periodic recalibrations by the auxiliary checkout system.

13.4.3 Stability of the Holographic Monitor

In the type of holographic monitor considered here, stability is dependent chiefly upon the following factors:

(1) Stability in the phase sensing electronics.
(2) Stability in the figure of the secondary mirror.
(3) Stability in the radial dimensions of the primary mirror.

Factors (1) and (2) affect the telescope performance directly. Factor (3) is indirect and somewhat less critical but in the present absence of experimental data it must be assumed that long-term radial creep in a large mirror blank may be substantial. Occasional checkout against a stellar wavefront analyzer is therefore highly desirable.